Author
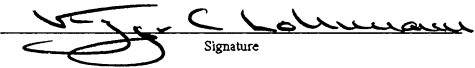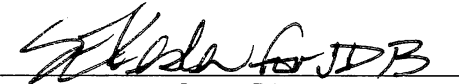
Elizabeth A. Smith

Title

A PETROGRAPHIC AND GEOCHEMICAL STUDY OF PERMIAN CARBONATES: IMPLICATIONS FOR THE Mg/Ca RATIO OF PERMIAN SEAWATER

submitted in partial fulfillment
of the requirements for the degree of
Master of Science in Geology
Department of Geological Sciences
The University of Michigan

Accepted by:

Signature	Name	Date
(signature) Signature	Dr. Kyger C. Lohmann	12-6-05
(signature) Signature	Dr. Bruce H. Wilkinson	12-6-05
(signature) Department Chair	Dr. Joel D. Blum	12/8/05

Table of Contents

ABSTRACT

A detailed petrographic and geochemical study of marine cements from the Permian Reef of New Mexico and West Texas was undertaken to test the hypothesis that the elemental chemistry of Permian seawater was similar to today's seawater. It has been proposed that the Mg/Ca ratio of seawater has varied over Phanerozoic time, resulting in alternating periods of predominantly aragonite versus calcite precipitation. The Permian reef contains abundant former aragonite and isopachous marine cements, which may have been formed at a time of a high Mg/Ca ratio of seawater, perhaps similar to today's ratio of 5:1. Isopachous marine cements collected from the Permian Reef Complex revealed microdolomite inclusions under SEM, indicating a mineralogy of former magnesian calcite. Previous studies of the Permian reef have shown that primary $\delta^{18}O$ and $\delta^{13}C$ isotopic values of these marine cements can be retained, and where they are preserved, elemental data should be able to be reconstructed, allowing for a calculation of the Mg/Ca ratio of Permian seawater. Well preserved samples were distinguished through a combination of petrographic, isotopic, and elemental data. The Mg content of well preserved samples show some variation, with samples from a neptunian dike and from crinoids showing the highest amounts of Mg. The variation in Mg content indicates that isotopically preserved samples might not be preserving their elemental content. Using a calculated distribution coefficient of 0.023 based on the estimated depth and temperature of precipitation of these former magnesian calcite cements, a range of 0.870 to 2.91 for the Mg/Ca ratio of Permian seawater was obtained from marine cements. The neptunian dike, at a Mg/Ca ratio of 2.60 may be the most reasonable estimate. These estimates for a Permian Mg/Ca ratio are much lower than fluid inclusion data from the same time period, and more work is needed to find out why this is the case.

INTRODUCTION

Most marine carbonate cements form directly from seawater, and therefore, can contain records of the Earth's oceans through geologic time. However, these cements are often composed of minerals that are metastable, such as high-magnesian calcite (HMC) and aragonite, and so are subject to diagenetic alteration. Investigating how much of the original features are preserved in a carbonate cement allows for the characterization of the original composition of the fluid from which the carbonate formed. From this, questions such as the reconstruction of ancient seawater chemistry, and inferring changes in the earth processes that control this chemistry, are possible.

Increasing evidence over the past several decades indicates that the mineralogy and minor element composition of different mineral phases precipitated

from seawater have varied over Phanerozoic time. Based on the mineralogy of early marine cements and ooids, Sandberg (1983) divided the Phanerozoic into intervals of "aragonite seas" and "calcite seas." Variations in atmospheric CO_2 and icehouse/greenhouse climate conditions were initially suggested as controls on these mineralogic changes (Sandberg, 1983). More recently, it has been suggested that this change in the composition of carbonate phases reflects primary changes in the Mg/Ca ratio of seawater as a result of variation in mid-ocean ridge hydrothermal activity (Hardie, 1996; Stanley and Hardie, 1998; Cicero and Lohmann, 2001). Changes in ocean water Mg/Ca have been inferred from studies of marine evaporite assemblages (Hardie, 1996), evaporated seawater contained in primary fluid inclusions in marine halites (Lowenstein et al., 2001; Horita et al., 2002), abiotic carbonate phases (Carpenter and Lohmann, 1992; Cicero and Lohmann, 2001), and biotic assemblages (Dickson, 2004). From these studies, it has been suggested that marine carbonate mineralogy is dominated by aragonite and HMC at low latitude reefal settings during periods of elevated seawater Mg/Ca.

In spite of the many studies conducted within the last decade, collective knowledge of the Phanerozoic evolution of seawater compositions based on elemental ratios in marine carbonate cements remains incomplete in that materials representing the critical time intervals of aragonite precipitation, when the Mg/Ca ratio of seawater is suspected to be similar to today's ratio of 5:1, have not yet been examined in detail. Carbonates formed within the massive, reefal facies of the Permian Reef complex of New Mexico and West Texas contain well-preserved marine cements, precipitated under proposed "aragonite sea" conditions. This

2

provides a unique locality in which to characterize seawater chemistry during a time of predominantly aragonite and high-magnesian calcite precipitation. Therefore, elemental and isotopic chemistry of carbonate cements from the Permian Reef complex allow for an opportunity to test the hypothesis that the Mg/Ca ratio of seawater was high during this period, and that Permian ocean chemistry was similar to today's oceans. An estimate of original seawater chemistry from the Permian would not only add to the information gained from studies of other Paleozoic carbonates (which have focused on times of "calcite seas"), but will also be compared to modern seawater chemistry, in which aragonite is the dominant abiotic carbonate phase in low latitude reefal settings. Marine carbonate precipitates are ideal to study because they can provide a more direct way to measure Mg/Ca ratios, and because abiotic carbonate cements are not plagued with the difficulties involved with potential vital effects from biotic material.

GEOLOGIC SETTING

Delaware Basin Formation

Late Paleozoic deformation of North America produced a series of basins that covered much of the present-day southwestern United States, including the Delaware Basin, located in New Mexico and West Texas (Adams, 1965). The Delaware Basin, which was formed during this deformational event, was once part of the much larger basin, the Tobosa Basin (Adams, 1965; Hills, 1984). During the late Mississippian through the Early Permian, the collision of Laurasia and Gondwana to form the supercontinent Pangea produced the Ouachita orogeny in the Marathon-

Delaware Basin region (Kluth and Coney, 1981). The consequences of this collisional event caused reactivation of PreCambrian basement, and block faulting. Consequently, the Central Basin Platform was uplifted, dividing the Tobosa Basin into the Delaware and Midland Basins (Hills, 1984). The Delaware Basin subsided rapidly during the Pennsylvanian in response to the Ouachita orogenic front, and remained a deep-water basin until the end of the Permian (Ye et al, 1996). During the Permian, the Delaware Basin was situated in a near-equatorial position along the western edge of Pangea and reefs began to form along the margin of the basin (Hill, 1996)

Capitan Reef Complex

Adams et al. (1939) was the first to divide the Permian into the Wolfcampian, Leonardian, Guadalupian, and Ochoan stages based on index fossils. In addition to the use of fusilinid biostratigraphy and lithological correlations, bentonites have provided an additional way to determine equivalent Guadalupian stata (Garber et al., 1989). During the Leonardian, small patch reefs formed, which set the stage for more extensive reef growth in the Guadalupian (Hill, 1996). The Goat Seep Reef formed during the Middle Guadalupian time, whereas the more extensively studied Capitan Reef Complex occurs in Upper Guadalupian strata. The Capitan Reef Complex outcrops along the southeast margin of the present-day Basin and Range block-faulted Guadalupe Mountains of New Mexico and West Texas (McKnight, 1984) (Fig. 1). The Capitan Limestone has been extensively studied, as it is one of the best exposures of a fossil reef in the world. Numerous canyons cut

perpendicular to the northeast-southwest trend of the Guadalupe Mountains, providing excellent exposures of the reef complex.

Lloyd (1929) was one of the first researchers to interpret the Capitan Limestone as a fossil reef, and noted that lateral changes in rock lithologies represented a transition of facies from backreef to reef, forereef, and basin. Many other researchers such as Kendall (1969), Cys et al. (1977) and Garber (1989) have all expanded on the facies concept, and what each facies represents. The Middle Guadalupian facies consist of the backreef Grayburg and Queen Formations, the Goat Seep Dolomite, and the basinal Cherry Canyon Formation. The Upper Guadalupian facies are composed of the backreef Seven Rivers, Yates, and Tansill Formations, the reefal Capitan Limestone, and the basinal Bell Canyon Formation (Fig, 2).

Major facies of the backreef region include the coastal sabkha/ playa made up of red siltstones, gysum and dolomite, and the tidal flat/ lagoon which contains mostly dolomite and evaporates. The lack of fossil diversity in the shelf facies indicates elevated salinities (Babcock, 1977), and the presence of the alga *Mizzia* indicates shallow water conditions (Kirkland and Chapman, 1990). A pisolite shoal characterized by pisolitic dolomitic limestones and tepee breccias may represent the shallowest position of the reef, although this is contested (Kirkland-George, 1992). The reef facies consists of an organic framework of calcareous sponges, algae, bryozoans, and other organisms bound together with inorganic cements to make a wave-resistant structure (Babcock, 1977; Yurewicz, 1977). The forereef had a steep slope, and consisted of mainly debris talus from the reef facies. The forereef grades

into the basinal facies, which consists of siltstones and sandstones that interfinger with limestone and dolomite.

The Capitan Limestone, which, along with equivalent shelf and basinal sediments, makes up the Upper Guadalupian strata, consists of a massive reef member that forms unbedded steep cliffs, and a thickly bedded forereef member. The Capitan Limestone is underlain by the older Goat Seep Dolomite (Crawford, 1989) and extends basinward beyond the Goat Seep Dolomite, indicating that the Capitan Limestone prograded laterally during its development (Hill, 1996). The massive reef member is primarily composed of boundstone lithologies, which contain the framebuilding problematical (algal?) genera *Tubiphytes* and *Archaeolithoporella*, calcareous sponges, and bryozoans, and abundant cement (Mruk, 1985). There is a diverse marine fauna in addition the framebuilding organisms which include brachiopods, fusilinids, bivalves, gastropods, ostracodes, echinoderms, cephalopods, trilobites, and corals, suggesting a normal marine environment (Babcock, 1977). Yurewicz (1977) found that the lower and middle parts of the massive facies may have formed in relatively deep water with low turbulence based on a lack of fossil zonation, however Babcock (1977) suggested a shallower origin for the upper part of the massive facies based on differing ecologic communities. The forereef member of the Capitan Limestone is also called the talus member since it contains boundstone debris derived from the reef (Kendall, 1969). The debris was probably emplaced by rockfalls, submarine slumps, slides, turbidity currents, and debris flows (Melim and Scholle, 1989). The forereef member shows patchy dolomitization (Mruk, 1985). Yurewicz (1977) divided the Capitan Limestone

into the lower, middle, and upper Capitan corresponding to the Seven Rivers, Yates, and Tansill Formations, respectively. The lower Capitan records a rapid progradation of the reef into the basin; whereas, the middle and upper Capitan shows more of an aggradation, with a steepening slope margin and decrease in debris to the basin. By Tansill time, evidence points to an increase in evaporative conditions and salinity, which resulted in the end of reef formation (Hill, 1996). The demise of the Capitan reef may have been due to increased climate aridity, restricted circulation of marine waters as the Hovey channel became cutoff, or uplift and exposure of the reef (Garber et al, 1989).

PREVIOUS RESEARCH

Petrography

The petrographic relationships of the marine cements within the Capitan Reef Complex have been extensively studied. Yurewicz (1977) and Mazzullo and Cys (1977) defined the cements present in the Capitan Reef, and subsequently Mruk (1985) and Given and Lohmann (1985) petrographically refined these definitions. Overall, there are three major cement types: botryoidal fibrous, isopachous fibrous, and equant spar. The botryoidal fibrous and isopachous fibrous are interpreted to have formed in a synsedimentary environment because they are intergrown with algal coatings and marine sediments (Yurewicz, 1977). The botryoidal fibrous cements occur as void-filling botryoidal arrays, or nodular growths associated with the problematical alga, *Archaeolithoporella* (Yurewicz, 1977). Based on the acicular nature of the fibrous arrays and on the basis of their optical properties and blunt

7

terminations, the botryoidal cements are interpreted to have precipitated as an original aragonite composition (Yurewicz, 1977; Mazullo and Cys, 1977; Mruk, 1985). The former aragonite cements locally comprise up to 80% of the carbonate in the Upper Capitan massive facies (Given and Lohmann, 1985; Mruk, 1985). Isopachous cements, which comprise radial fibrous (and possibly fasicular optic, Rahnis and Kirkland, 1999), radiaxial fibrous and prismatic cements occur as layers of light to dark brown crystals which uniformly coat the substrates on which they precipitate, and are interpreted to have formed either after the aragonite cements (Mruk, 1985), or potentially deeper in the reef . Based on the presence of radiaxial extinction and microdolomite inclusions, these isopachous cements are interpreted to have been precipitated originally as magnesian calcite cements (Lohmann and Meyers, 1977; Mruk, 1985; Given and Lohmann, 1985).

Under cathodoluminescent microscopy, both the former aragonite and magnesian calcite cements show a patchy mixture of areas of luminescence and nonluminescence (Mruk, 1985; Given and Lohmann, 1985). As the quality of preservation deteriorates, luminescence increases, indicating that diagenesis of these cements has resulted in a mixture of a luminescent and nonluminescent phases, which form a linear covariant trends in stable carbon and oxygen isotope plots. The convergence of trends from samples taken along an Upper Capitan paleoslope allowed Given and Lohmann (1985) to derive an average original isotopic composition of the nonluminescent phase based on former aragonite samples of -2.5 ‰ $\delta^{18}O$, and + 5.3 ‰ $\delta^{13}C$. The marine isotopic signature remained constant throughout the reef and foreslope facies, indicating that the Delaware Basin

was a well mixed water mass. However, there is an enrichment in $\delta^{18}O$ towards the end of the Guadalupian, which suggests increased restriction of the Delaware Basin.

After cementation of the reef by aragonite and magnesian calcite cements, much of the remaining porosity was filled by clear, equant sparry calcite cements. Under cathodoluminescence, these cements show alternating nonluminescent and brightly luminescent couplets, which may be related to more rapid oxidizing flow and decreased flow with more reducing conditions, respectively (Mruk, 1985). Based on the relatively constant oxygen isotope composition and the enrichment in carbon isotopic composition with increasing paleodepth, Given and Lohmann (1986) concluded that Spar I represents the establishment of a meteoric-phreatic system in the reef facies. Mruk (1985) and Crysdale (1986) suggest that Spar II was precipitated in an elevated temperature regime in a burial phreatic system. More recently, Hill (1996) believes that Spar II is related to the uplift of the Basin and Range instead of burial.

Preservation of the Capitan Reef Complex

Prior work by Given and Lohmann (1985, 1986) has demonstrated that primary marine $\delta^{13}C$ and $\delta^{18}O$ isotopic compositions can be obtained from these ancient cements through detailed petrographic and geochemical analyses. In the Permian Reef Complex, both former aragonite and magnesian calcite cements were examined. Given and Lohmann (1985) showed that microsampling of the mixture of luminescent and nonluminescent phases produces linear covariant trends which converge at primary marine cement values. Interestingly, the former aragonite and

9

high-magnesian calcite cements converge at differring primary marine values with an offset similar to modern aragonite and high-magnesian calcite cements, indicating that the primary marine values of both mineral phases were in fact preserved during diagenesis. The original marine value is for high-magnesian calcite is shown to have a $\delta^{18}O$ of -2.7 ‰ and a $\delta^{13}C$ of 4.3 ‰ (Carpenter and Lohmann, 1997). Where oxygen isotopic compositions of the marine cements are preserved, water/rock ratios can be inferred to have been very low (i.e. a "closed" system), and so stabilization under closed system conditions allows the original marine isotopic values of the dissolving phase to be imprinted on the secondary diagenetic phase which was isolated from exchange with external secondary fluids.

METHODS

Field work was conducted during the summer of 2004, and consisted of sampling from the massive reefal facies of the Permian Reef Complex in New Mexico and West Texas. Samples were taken from both Bear and McKittrick Canyons. Slabs were cut from each sample, polished, and diamond polished thin sections of the areas with the highest density of isopachous cements were made. The thin sections of Permian marine cements were examined by polarizing and cathodoluminescence microscopy to distinguish between primary marine components and later diagenetic phases. Cathodoluminescence microscopy was performed on a Technosyn cold cathodoluminescent Model 8200 Mk II unit at 15 kV with a 150-450 μA beam current.

Samples deemed well preserved from cathodoluminescent microscopy were selected and carbon-coated for scanning electron microscopy analysis. Analysis was undertaken using a Hitachi S3200 SEM to locate microdolomite inclusions in isopachous marine cements using backscatter electron images to support an origin of high-magnesian calcite for these cements. The SEM was also used to characterize the distribution and shape of the microdolomite inclusions, as well as to give a qualitative idea as to their chemical composition. Crinoids, where present, were also analyzed. The leaching technique of Glover (1961) was used to etch the polished surface of one thin section with cold 0.17 M EDTA to develop slight relief such that microdolomite inclusions would stand out. In subsequent samples that were not etched with EDTA, it was determined that etching was not necessary to reveal the inclusions on BSE images. Volumes of microdolomite inclusions in isopachous cements and crinoids were estimated using a computer imaging program which quantified areas in the BSE images according to their gray-level scale. Back-scattered electron imaging obtained during scanning electron microscopy work helped to determine the best sampling techniques for the magnesian calcite cements for isotopic and elemental analysis.

Two sampling techniques were utilized during this study to obtain carbonate material for geochemical analyses. Initially, bulk samples were drilled from areas of isopachous marine cement on polished rock chips using a microscope-mounted drill assembly. Bulk samples were acquired first to resolve which samples would be best utilized for more precise sampling. These analyses established an overview of the $\delta^{13}C$ and $\delta^{18}O$ isotopic variation as well as the elemental variation of Sr, Mg, Mn, Fe,

and Ca in the reefal sequence. High-resolution sampling was performed using a Merchentek Micromill on diamond polished thin sections of selected rock chips. Sample areas were digitized and drill paths interpolated along areas of isopachous marine cement that showed the least luminescence under cathodoluminescence evaluation. A computerized X-Y-Z stage was used to mill out the interpolated drill paths.

Approximately equal size splits of carbonate powder from the bulk samples and high-resolution samples (~20 μg each) were taken for stable isotope and elemental analyses. Samples taken for stable isotope analysis were roasted in a vacuum at 200°C for one hour to remove volatile contaminants and water. Samples were then reacted at 76° ± 2°C with anhydrous phosphoric acid in a Finnigan MAT Kiel device coupled to a Finnigan MAT 251 isotope-ratio mass spectrometer. Isotopic ratios were corrected for ^{17}O contribution and adjusted for acid fractionation and source mixing by calibration to a best-fit regression line defined by the standards NBS-18 and NBS-19. Precision of the data is better than 0.1% for carbon and oxygen isotopes, and is maintained through daily analysis of carbonate standards. All stable isotope data are reported in ‰ notation relative to VPDB.

Splits of the identical sample powders used for isotopic analyses were measured for Mg, Ca, Sr, Mn, and Fe contents using a High Resolution Finnigan Element ICP Mass Spectrometer. Powdered samples were dissolved in 1.2 ml of dilute 1% HNO_3 plus 2% HCl spiked with Indium as an internal standard. Samples were then further diluted with 1% HNO_3 diluted with Indium as an internal standard. Paired isotopic and elemental analyses are important, as the preservation of

elemental chemistry is based on the retention of primary isotopic values. Precision of the elemental analyses were better than 2%, and precision of the Mg/Ca ratios were better than 0.3%.

Electron microprobe study allowed for the differentiation and analysis of microdolomite inclusions versus the surrounding calcite cement in former magnesium calcite cements and crinoids through spot analyses of the inclusions and calcite. Microdolomite inclusions and the surrounding host calcite were randomly sampled with the same operating conditions to allow comparison of these two components. Concentrations of Ca, Mg, Mn, Fe, and Sr were determined on a Cameca SX100 microprobe with an accelerating voltage of 15 kV, beam current of 4 nA, a beam diameter of 2 μm, and a counting time of 10 s. Detection limits were 1670 ppm for Ca, 600 ppm for Mg, 1430 ppm for Fe, 1400 ppm for Mn, and 3580 ppm for Sr. Analysis of these isopachous cements on the electron microprobe provided a crucial check on the data obtained from the ICP-mass spectrometer.

RESULTS

Examination of isopachous marine cements under a polarizing microscope revealed that the cements form layers of cloudy gray to brown crystals which uniformly coat the surfaces where they precipitate. Isopachous cements often coat fossil materials such as *Archaeolithoporella*, *Tubiphytes*, bryozoans, brachiopods, sponges, and fusilinids. Isopachous cements were also seen to coat aragonite botryoids. Most crystals observed displayed radiaxial-fibrous optical properties, in which twin planes, where visible, were curved concave-upwards towards the tip of

the crystal, and undulose extinction in which the extinction direction migrated in the same direction as which the microscope stage was turned. Radiaxial-fibrous calcite is unique in that it has been associated with former high-magnesian calcites (Lohmann and Meyers, 1977).

Differing optical properties were seen in other areas of the isopachous cements. Small areas within the cement or certain layers within a continuum of isopachous crystals displayed radial-fibrous or fasicular-optic extinction properties. In most cases, fasicular-optic crystals were initially observed, in which undulose extinction migrated in the opposite direction of the way the microscope stage was turned. On closer examination, the fasicular-optic crystals resolved themselves into smaller crystals, each with radial-fibrous properties (straight twin planes and unit extinction). Thus, it seems that the radial-fibrous crystals were in the process of coalescing to form fasicular-optic calcite, although these two crystal forms were much rarer overall than radiaxial-fibrous calcite.

Under cathodoluminescent microscopy, isopachous calcite cements displayed a range of properties based on their level of preservation. Well preserved cements showed a relatively dark, but still dull orange luminescence. As preservation levels decreased, the dull orange luminescence became brighter, and interspersed with small brightly luminescent orange areas, imparting a patchy, or blotchy appearance to the calcite. Some samples showed alternating layers of bright orange luminescence and dark dull orange luminescence. Poorly preserved cements displayed large areas of bright red luminescence indicating secondary dolomite overgrowth. The crystal terminations in the isopachous layers display a

14

progression of probable meteoric alteration, as larger crystals grade into even larger calcite spars with alternating bands of bright orange luminescence and nonluminescent layers. More poorly preserved isopachous cements often show large red rhombic dolomite crystals at the termination of calcite crystals (Fig. 3 and Fig. 4).

Crinoids were not especially numerous in samples from the Permian Reef. However, where present, crinoids were easily identifiable under polarizing microscopy by their generally larger size than other skeletal material, and the unit extinction of their crystals. Under cathodoluminescence, crinoids were most often nonluminescent. They were very easily identifiable under cathodoluminescence because they were usually the only completely nonluminescent component in thin section. Occasionally, a crinoid was brightly luminescent, or had a nonluminescent core with a luminescent outer layer. Nonluminescent crinoids were taken to be the least altered, and were further analyzed (Fig. 5).

SEM studies revealed that the inclusions were dolomite in composition, and that overall, microdolomite inclusions were more numerous in the crinoids than in the former magnesian calcites. The cements contained mostly anhedral to subhedral dolomite inclusions which ranged in size from 5-30 μm across. In some samples the size of the dolomite inclusions were about the same average size, however in other samples there was a large variation in the size of the inclusions (Fig. 6). Dolomite that was clearly from an external fluid source occurred at the outer edges of the cements and was much larger, at over 100 μm across. In general, microdolomite inclusions tended to occur in bands or in patches in the isopachous cements,

although their distribution in selected samples, such as one from a neptunian dike in McKittrick Canyon, was more uniform. Volumes of microdolomite inclusions overall ranged from 0.460% to 6.86%, with a mean of 3.46%. The neptunian dike showed the highest density of all the samples, at over 6.00% (Fig. 7A, 7B).

Microdolomite inclusions in the crinoids were more numerous and more uniformly distributed than those in the isopachous cements. The inclusions were approximately equal in size to those in the isopachous cements; however, in some cases the inclusions were more subhedral than anhedral. This was the case with most of the crinoids observed, however there was one sample in which some stereom structure was visible, and the microdolomite inclusions were not well developed into rhombic crystals but dolomite was found in and around the stereom structures. The range in volume of microdolomite inclusions in the crinoids examined was 8.38% to 17.1%, with a mean of 13.4%.

Porosity in most of the marine cement and crinoid samples was approximately 5%. This porosity was not accounted for in volume estimates of microdolomite inclusions, meaning that the porosity was assumed to contain calcite. In fact, some microdolomite inclusions were probably present in at least some of the current pore space. It is difficult to know exactly how much of the porosity was occupied by dolomite, and so we can only say that estimates of microdolomite volumes are minimum estimates only, with actual amounts of microdolomite slightly higher.

Microprobe analysis of the inclusions and surrounding calcite in the isopachous cements and crinoids revealed that magnesium was concentrated in the

inclusions in both components. No appreciable magnesium was found in the surrounding host calcite, indicating that it is indeed a low-magnesium calcite. A 48-50 mole % magnesium occurred with highest frequency in the microdolomites found in isopachous cements (Fig. 8). Some microdolomites had a lower magnesium content, which is probably because they were located under a thin layer of calcite, as indicated by the fact that some inclusions appeared to not be in focus while surrounding inclusions were in focus under the BSE viewer. Magnesium content of crinoids also revealed a 48-49 mole % magnesium with highest frequency. The slight calcium enrichment of the microdolomite inclusions is probably an artifact of the microprobe analytical procedure related to vaporization of CO_2 from the surrounding carbonate (see Lohmann and Meyers, 1977).

The stable carbon and oxygen isotopes of the former magnesian calcite cement show a similar linear covariant trend to that of Given and Lohmann (1985) when plotted together (Fig. 9). The cement from Bear Canyon displayed two linear covariant trends. The upper trend follows a linear path from the proposed Permian original marine value at a $\delta^{18}O$ of -2.7 ‰ and a $\delta^{13}C$ of 4.3 ‰ towards Spar II at about -12 $\delta^{18}O$. The data points along this trend indicate mixing between one calcite phase that retains the original Permian $\delta^{18}O$ and $\delta^{13}C$ marine values and Spar II, which probably involves a deep burial fluid. The lower trend from Bear Canyon also follows a linear path which begins at the original marine value but slopes steeply down towards Spar I at -8 ‰ $\delta^{18}O$. Spar I may be meteoric in origin (Given and Lohmann, 1986). Stable isotopes from McKittrick Canyon also show a linear covariant trend, however this trend does not extend nearly as far towards the

17

calcite spars as does the trend from Bear Canyon, which probably reflects the extent of sampling from McKittrick Canyon. Although more of the data from McKittrick Canyon are clustered around the original Permian marine value, the trend extends above the original marine value to a slightly heavier carbon value. Many of the samples with more positive carbon also contain elevated iron contents, indicating that they may be diagenetically altered, and not reflect the original isotopic composition of Permian marine water.

The elemental data confirm that the former magnesian calcite cements chosen for sampling, which have a dark dull luminescence, have low levels of Mn overall (Fig. 10 and Fig. 11). The Fe content is variable, with more well preserved samples presumably having lower amounts of Fe. A clustering of samples with a Fe/Ca (mmol/mol) content of less than 0.150 was used as an indicator of more well-preserved samples. Samples that fell into this grouping were used to calculate a Mg/Ca ratio of Permian seawater. Marine cements showed variable amounts of magnesium, but most commonly values ranged between 1.0-3.0 mole % $MgCO_3$. Samples from the neptunian dike showed the highest magnesium content, at the upper range of values. Crinoids in general had much more magnesium than the cements, with values ranging from 3.0-6.0 mole % $MgCO_3$.

The elemental Mg contents obtained from the ICP-MS correspond well to the volumes of microdolomite estimated from BSE images. To convert from a mole % $MgCO_3$ to a volume of dolomite, it must first be noted that the formula for dolomite is $Ca_{0.5}Mg_{0.5}CO_3$. If a magnesian calcite rock containing 10 mole % $MgCO_3$ and 90 mole % $CaCO_3$ dissolves and reprecipitates to form dolomite and calcite, then for

every dolomite formed, 0.5 moles of Mg goes to the dolomite formation, and there is 9.5 mole % $MgCO_3$ left. As dolomite is progressively formed, 20 units of dolomite can be formed from a 10 mole % $MgCO_3$. Thus, doubling the mole % $MgCO_3$ of a sample should give an estimate of the volume % of microdolomites it should contain. As an example, the neptunian dike contained approximately 6.0 volume % microdolomite inclusions, and thus contained 3.0 mole % $MgCO_3$ when examined with the ICP-MS. Likewise, crinoids contained an average of about 13 volume % microdolomite inclusions, and had a 6.0 mole % $MgCO_3$.

Sr data showed two distinct linear trends on a Sr/Ca versus Mg/Ca plot. Interestingly, samples mostly from McKittrick Canyon, with the exception of one sample from Bear Canyon, plot on the top trend containing elevated amounts of Sr. The bottom trend contains samples solely from Bear Canyon. Regression lines through each of these trends yield regression coefficients of only 0.34 and 0.39, with Sr/Mg slopes of 0.0025 and 0.0009, respectively. These Sr/Mg values are much lower than estimates from other time periods in the Phanerozoic (Cicero and Lohmann, 2001).

DISCUSSION: The Mg/Ca Ratio of Permian Seawater

Geochemical Models

Geochemical models have been proposed for the entire Phanerozoic which predict that the Mg/Ca ratio of seawater varied between 1.0 and 5.0 throughout this time (Wilkinson and Algeo, 1989; Hardie, 1996). These oscillations also coincide with other global cycles such as sea level, icehouse versus greenhouse conditions,

and atmospheric CO_2. The Hardie (1996) model uses estimates of the supply of Mg and Ca to the ocean by rivers, exchange of these elements by hydrothermal fluids generated at mid-ocean ridges, and removal of these elements by precipitation of carbonates and evaporites. A major sink of Mg^{2+} is dolomitization, which is incorporated into some models, although estimates of dolomite abundance through time can vary (Holland and Zimmermann, 2000).

Geochemical model estimates for the Mg/Ca ratio of seawater from the Permian differ. The Hardie (1996) model, which is based on variations in ocean crust production as estimated by the Phanerozoic sea level curve, shows multiple small-order oscillations during the Mississippian through Jurassic time, with Mg/Ca ratios falling from a high of 4.5 during the late Pennsylvanian/early Permian to a low of 3.0 during the late Permian. Mg/Ca values rise slightly at the end the Permian/beginning of the Triassic up to 3.5. The Wilkinson and Algeo (1989) model shows a similar high in Mg/Ca during the early Permian, however the magnitude is lower, at only about 2.8. Mg/Ca then falls during the late Permian/lower Triassic to 1.0. Thus, it is evident that estimates from the Permian vary widely, with values as high as 4.5 to values which drop to as low as 1.0. However, for the majority of Permian time, the two models seem to agree that the Mg/Ca ratios appear to have been higher than other times such as earlier in the Paleozoic, with values most likely around 3.0.

Fluid Inclusions and Evaporite Mineralogy

Modern evaporated seawater produces brines which are depleted in the concentration of Ca^{2+}, and which are considered $MgSO_4$ rich. Sedimentary basins such as the U.S. Gulf Coast contain volumes of brine at depth with high concentrations of Ca^{2+}, and are distinct from modern seawater. Since evaporative concentration of modern seawater results in brines depleted in Ca^{2+}, this suggests that these different basinal brines inherited their chemistry from evaporated seawater formed during times when oceans were enriched in Ca^{2+} and depleted in SO_4^{2-} (Lowenstein et al., 2003). Geologic periods, such as the Permian, which have elevated magnesium ion and sodium ion concentrations coincide with periods when aragonite and $MgSO_4$ salts were important marine precipitates. In contrast, periods where the Mg/Ca ratio of seawater is less than 2 coincide with times when seawater was depleted in Mg and Na, calcite is the dominant carbonate precipitate, and evaporites contain K, Mg, and Ca chloride salts (Lowenstein et al., 2001). Hardie (1996) has compiled data which indicate that times when aragonite cements are abundant coincide with the presence of $MgSO_4$ evaporite deposits; whereas when calcite is the predominant abiotic precipitate, KCl evaporites are precipitated.

Fluid inclusions within halites of these evaporite deposits have also been used to reconstruct ancient seawater chemistry; however, there can be problems involved when using these ancient fluid inclusions. First, the brines trapped as inclusions may or may not be derived from seawater. The inclusions may record the ancient seawater chemistry, or they may be the result of what is termed syndepositional recycling, a process in which meteoric water inundates the basin

thereby dissolving the original salts (Timofeeff et al., 2001). Inclusional brines are also not simply the parent seawater concentrated into the brine because of the precipitation of minerals during brine evolution. Modeling techniques must be used to extrapolate and back-calculate the individual ion compositions of ancient seawater. These techniques can be complicated both from the addition of external waters and from effects of dolomitization (Timofeeff et al., 2001).

Horita et al. (1991) studied brine inclusions in marine halite from the Permian Salado Formation in the Delaware Basin and found that the composition of Permian seawater was probably similar to modern seawater. Horita et al. (2002) expanded on these studies and found that at a minimum, the magnesium ion concentration of Permian seawater was 48 mmol/kg H_2O. Since some of the inclusional brines have been modified by in-basin dolomitization, the magnesium content is only a minimum estimate. Estimates of the sulfate ion concentration were 16 mmol/kg H_2O at a minimum, and calcium ion content was a minimum of 14 mmol/kg H_2O. Horita et al. (2002) translated their data into an estimate of the Mg/Ca ratio of Permian seawater to be similar to today's, at 5.2. Lowenstein et al. (2001) also found that the composition of fluid inclusions in marine halites from the Permian most closely resembled modern seawater. Calculated Permian Mg/Ca ratios were always higher than 2.5, and sometimes higher than 4.

Echinoderm Data

Dickson (2002, 2004) has investigated the use of echinoderms in reconstructing ancient seawater chemistry. Although in the past echinoderms have

not been used as potential proxy for marine Mg/Ca ratios because of their susceptibility for diagenetic alteration, echinoderms, like some marine cements, have the potential for closed-system diagenesis, and can alter from a high magnesian calcite to a mixture of calcite and dolomite that preserves the original bulk composition. It appears that the Mg^{2+} composition of marine echinoderms rises and falls in phase with the other Phanerozoic oscillations in Mg/Ca predicted by others (Dickson, 2004).

Although Dickson's echinoderm data generally follow the trends set by others for the Mg/Ca ratio of seawater over time, the echinoderm data differ substantially when changes over shorter time intervals are considered. Prediction of seawater Mg/Ca ratios from echinoderms also has disadvantages as Mg partitioning during growth of the echinoderm is not understood well, and therefore accurate prediction of the Mg/Ca ratio of seawater is uncertain. Even when modern echinoderms have been examined, it appears that different parts of an echinoderm partition Mg differently than other parts (Ries, 2004). Even if a distribution coefficient of Mg for modern echinoderms could be reliably calculated, this distribution coefficient could be very different for differing species of echinoderms in the past. Care must also be taken to minimize the possibility that crinoids examined were not formed in colder waters, as this would also affect Mg partitioning. Diagenetic alteration of the crinoids also must be examined in detail as to assure closed-system diagenesis. Under cathodoluminescence, crinoids that have been altered are more readily seen as highly luminescent. Crinoids can show varying amounts of luminescent intergrowth under cathodoluminescence, and analysis of Mg contents of a brightly luminescent

crinoid would result in an inaccurate assessment of how much Mg may have been present in the crinoid before it was altered.

Data from the Upper Permian from echinoderms reveal averages of 7.7, 8.5, and 9.6 mole % $MgCO_3$. The range, however, is quite large, spanning from approximately 6.5 to 13 mole % $MgCO_3$ (Dickson, 2004). This translates into average estimates of the Mg/Ca ratio of seawater for the Permian to be 2.2, 2.5, and 2.9, with a range from 1.5-2.5. These estimates are considerably lower than estimates from fluid inclusions of Permian age.

Estimating a Mg/Ca Ratio of Permian Seawater from the Permian Reef Complex

Since the isopachous marine cements of the Permian Reef show radiaxial extinction, and because of the presence of microdolomite inclusions revealed under SEM, these cements are most likely former magnesian calcite cements (Wilson and Dickson, 1996; Lohmann and Meyers, 1977). Since magnesian calcite is a metastable carbonate phase, there is a diagenetic drive towards the formation of more stable phases, namely calcite and dolomite. Thus, stabilization of magnesian calcite occurs through dissolution-precipitation reactions because of the metastability magnesian calcite, and because of the solubility differences between magnesian calcite, low-magnesian calcite (LMC) and dolomite. In a most likely scenario, trapped diagenetic fluids in the system dissolve the magnesian calcite, and precipitate stable LMC. When the Mg/Ca of fluid increases to point where magnesian calcite dissolution is inhibited, dolomite is precipitated, resulting in the formation of

24

microdolomite inclusions. In this manner, microscale dissolution of the magnesian calcite, followed by magnesium enrichment of the solution, followed by the precipitation of LMC and dolomite results in the diagenetic fabric of these former magnesian calcite Permian marine cements. Since these dissolution-precipitation reactions occurred in a closed system manner, as suggested by the preservation of primary marine isotopic signatures in the Permian Reef, elemental compositions of the calcite phases (namely magnesian calcite cement) should also be preserved. From the Mg/Ca of the former magnesian calcite cement, the Mg/Ca ratio of seawater can be calculated because the Mg/Ca of the mineral phase is related to the Mg/Ca of the liquid via the distribution coefficient of magnesium into calcium carbonate.

$$D_{Mg} = \frac{Mg/Ca_{calcite}}{Mg/Ca_{liquid}}$$

In order to calculate the Mg/Ca ratio of seawater, however, the best value for the Mg/Ca of the former magnesian calcite cements and the best distribution coefficient must be determined. The volume of microdolomite inclusions was determined through SEM studies. Assuming that a value of 6.0%, such as the values found from the neptunian dike represents a reasonable number for the volume percent of microdolomite inclusions, this would be equivalent to a magnesian calcite containing about 3.0 mole % $MgCO_3$. If these Permian marine cements were high magnesian calcite cements, there has been some magnesium lost. One would expect that if aragonite and high magnesian calcite cement are the most common abiotic precipitates during times of high seawater Mg/Ca, then the magnesian calcite cements of the Permian reef would also be of high magnesian calcite mineralogy,

but perhaps this is not the case. The presence of a later luminescent calcite phase visible under cathodoluminescence does account for some loss of Mg. Under cathodoluminescence it appeared that about half of the present volume of the isopachous calcites consisted of former magnesian calcite and the other half consisted of the younger luminescent calcite phase. This would indicate that the amount of magnesium present in the neptunian dike sample could be corrected from 3.0 mole % $MgCO_3$ to 6.0 mole %. This value agrees with the higher amounts of magnesium found in the crinoids, and may mean that magnesium has been lost from the former magnesian calcite cement but retained in the crinoids. This is supported by the presence of more microdolomite inclusions in the crinoids and the lack of luminescent intergrowth in the crinoids sampled.

Hasiuk (2005) analyzed crinoids and marine cements from Muleshoe Mound in the Mississippian Lake Valley Formation, and isolated nonluminescent crinoids as well as crinoids of varying luminescence for isotopic and elemental analysis. The nonluminescent crinoids were found to be isotopically and elementally similar to the marine cements. The crinoids also plot closer the original isotopic marine value for the Mississippian, indicating that they are well preserved. Luminescent crinoids appear to have lost Mg when they were diagenetically altered, indicating that nonluminescent crinoids from the Permian reef may record a Mg value that is more representative of the true Permian Mg/Ca ratio, however Mg partitioning in crinoids still remains problematic.

The low amount of magnesium found in the former magnesian calcite cements could also been explained by temperature. In modern environments,

higher magnesium incorporation into calcium carbonates occurs in shallow, warm, tropical settings, whereas calcites with lower magnesium contents occur higher latitudes, or at greater depths (i.e. colder temperatures) (Major and Wilbur, 1991). Abiotic marine calcites from modern shallow water tropical settings (25-29°C) contain 14-18 mole % $MgCO_3$, whereas at a depth of 200m, 14 mole % $MgCO_3$ form, and at temperatures of 15-20°C, 12-15 mole % $MgCO_3$ form (Videtich, 1985). Former magnesian calcite cements in the Permian Reef usually occur lower in the reef than aragonite cements, indicating that they formed at greater depths and/or temperatures. Based on estimates of water depth above the reef (Weidlich and Fagerstrom, 1999), reefal height, and where samples were collected, a maximum depth of precipitation of the magnesian calcite samples collected is about 200m, and so seawater temperatures were probably cooler where magnesian calcites were being precipitated.

In order to predict seawater Mg/Ca ratios from former magnesian calcite cement data, Mg^{2+} partitioning must be understood, which makes estimating a distribution coefficient (D) problematic. Laboratory studies can provide an understanding as to the factors which control magnesium incorporation into calcite, and this has been investigated extensively. It has been found that D_{Mg} values increase with increasing temperature and Mg/Ca of the solution, and decrease with increasing SO_4^{2-} (Katz, 1973; Mucci, 1987; Mucci and Morse, 1983; Mucci et al., 1989). The effect of precipitation rate and P_{CO2} on magnesium partitioning are still controversial (Given and Wilkinson, 1985; Burton and Walter, 1991; Mucci and Morse, 1983; Hartley and Mucci, 1996). Unfortunately, results of laboratory

experiments conducted at conditions similar to tropical reefal environments underestimate the observed composition of modern marine high magnesium calcites by 4-6 mole % $MgCO_3$ (Videtich, 1985; Burton and Walter, 1991; Hartley and Mucci, 1996).

Given the molar Mg/Ca ratio of seawater, Carpenter et al. (1991) estimated a mean distribution coefficient for Mg for modern abiotic calcite from Enewetak Atoll to be D_{Mg} = 0.034. Using this distribution coefficient, and a Mg/Ca molar ratio of the Permian marine cements of 0.06, we get a Mg/Ca ratio of only 1.76 for Permian seawater. Assuming that these former magnesian calcite cements formed in cooler waters, and assuming that today a HMC of 12 mole % $MgCO_3$ would form at a depth of 200m, using today's Mg/Ca ratio of 5.14, a distribution coefficient of 0.023 can be calculated. Using this modified distribution coefficient and applying it to the marine cement in the neptunian dike containing a modified mole % $MgCO_3$ of 6.00 (assuming a luminescent intergrowth of 50%), we come out with a Mg/Ca ratio of Permian seawater to be 2.60, which is obviously much lower than the Mg/Ca ratio of today's seawater. This estimate of 2.60 is also just about the highest estimate from the Permian reef. If we take the Mg/Ca ratios of the best preserved samples according to Fe content, meaning that samples containing more than 0.150 mmol/mol Fe are discounted, then estimates for the Mg/Ca of Permian seawater from former magnesian calcite cements range from 0.870 to 2.97, with an average of 1.50. These values were calculated with a D_{Mg} of 0.023. Crinoids were not numerous enough in the samples from the Permian reef to provide a solid estimate of Permian Mg/Ca, and they also grew closer to the ocean surface, which would

mean a different distribution coefficient must be used. Thus, the "best estimate" of 2.60 from a well-preserved neptunian dike sample seems to be on the high end of estimates for the Permian Mg/Ca of seawater, however if many of the samples are showing Mg loss, then perhaps a high estimate is reasonable (Table 1).

While the estimate of 2.60 is lower than the Mg/Ca ratio of today's oceans (at 5:1), it does fit with estimates from other studies. In fact, this estimate is similar to that of the geochemical models, which seem to agree around a value of 3.0 for the Permian. Estimates from crinoids also seem to agree, as Dickson's best averages give estimates of Permian seawater around 2.5, although the range is very great, which is somewhat troubling. Fluid inclusion Mg/Ca values seem to generally be higher than estimates from models, crinoids, and marine cements. Lowenstein (2001) revealed values that were always above 2.5, and sometimes higher than 4.0. Estimates from Horita et al. (2002) were even higher, at 5.2. Therefore, it seems that estimates from crinoids and from this study of marine cements reveal lower Mg/Ca ratios of Permian seawater than fluid inclusion data (Fig. 12). In such a case, either the crinoid and marine cement data are underestimating the Mg content of the Permian samples, or the fluid inclusion data are overestimating the amount of Mg present in their samples.

Since it has been shown that the marine cements from the Permian reef can retain their original isotopic composition, it was proposed that the isotopically well preserved samples should preserve their elemental values. Therefore, it seems that well preserved samples should show a more uniform Mg content, however there is a large variation in the amount of Mg, making it hard to decide on a reasonable Mg/Ca

ratio of Permian seawater from these marine cements. It seems that the crinoids retain more Mg, however it is unknown whether vital effects may have played a role in retention of Mg in crinoids. Thus, the estimate from marine cements of 2.60 for the Permian is not an absolute. And so, either the Permian seas did not contain as much Mg as might have previously been thought, or they may have contained high amounts of Mg, which are not retained by these marine cements or crinoids.

CONCLUSIONS

Well preserved samples of former magnesian calcite cement from the Permian Reef Complex were obtained by a variety of methods. Petrographically, those samples with the darkest luminescent properties under cathodoluminescence were isolated. Isotopically, those samples that plotted closest to the original Permian marine seawater value were considered. Finally, those samples with the lowest Fe content were isolated in order to calculate a Mg/Ca ratio for Permian marine seawater. Although there is still the potential for Mg loss and diagenetic alteration, the methods of sample selection tried to ensure picking samples with the lowest amount of alteration for calculation of the Mg/Ca ratio of seawater.

The calculation of a Mg/Ca ratio of Permian seawater involves further assumptions because there is an additional luminescent diagenetic phase present in the former marine cements, from which Mg has been lost. Therefore any estimates of Mg content will probably underestimate the amount of Mg originally present. This is why it was assumed that 50% of the original fabric has been replaced by a later luminescent calcite phase in calculations regarding the Mg/Ca ratio of seawater.

This assumption was also supported by the presence of nonluminescent crinoids which retained approximately 50% more Mg than the former marine cements. A further assumption is the value of the distribution coefficient used to calculate the Mg/Ca ratio of seawater. Since these former magnesian calcite cements most likely precipitated in deeper colder waters than the aragonite which precipitated in the warm surface waters of the reef, a distribution coefficient lower than 0.034 does not seem unreasonable.

Despite effectively increasing the Mg content of the samples based on the assumption that Mg has been lost and replaced by a diagenetic luminescent phase, the estimates for the Mg/Ca ratio of Permian seawater are still much lower than today's value. The range of 0.870 to 2.97, with a best estimate of 2.60 for the Mg/Ca ratio of Permian seawater for marine cements is also, for the most part, lower than most fluid inclusion estimates. The values do somewhat coincide with data from crinoids. This suggests that more research needs to be done to resolve these differences in estimates for the Permian for fluid inclusion data versus crinoid and marine cement data.

REFERENCES

Adams, J. E., Cheney, M. G., DeFord, R. K., Dickey, R. I., Dunbar, C. O., Hills, J. M., King, R. E., Lloyd, E. R., Miller, A. K., Needham, C. E., 1939, Standard Permian section of North America: American Association of Petroleum Geologists Bulletin, v. 23, p. 1673-1681.

Adams, J. E., 1965, Stratigraphic-Tectonic development of Delaware Basin: American Association of Petroleum Geologists Bulletin, v. 49, p. 2140-2148.

Babcock, J. A., 1977, Calcareous algae, organic boundstones, and the genesis of the Upper Capitan Limestone (Permian, Guadalupian), Guadalupe Mts., West Texas and New Mexico, in, Hileman, M. E., and Mazzullo, S. J. (eds.), Upper Guadalupian facies, Permian Reef Complex, Guadalupe Mountains, New Mexico and West Texas: 1977 Field Conference Guidebook, Permian Basin Section, SEPM Publication 77-16, p. 3-44.

Burton, E.A., and Walter, L.M., 1991, The effects of P_{CO2} and temperature on magnesium incorporation in calcite in seawater and $MgCl_2$-$CaCl_2$ solutions: Geochimica et Cosmochimica Acta, v. 55, p. 777-785.

Carpenter, S.J., Lohmann, K.C., Holden, P., Walter, L.M., Huston, T., and Halliday, A.N., 1991, $\delta_{18}O$ values, $^{87}Sr/^{86}Sr$ and Sr/Mg ratios of Late Devonian abiotic marine calcite: Implications for the composition of ancient seawater: Geochimica et Cosmochimica Acta, v. 55, p. 1991-2010.

Carpenter, S.J., and Lohmann, K.C.,1992, Sr/Mg ratios of modern marine calcite: Empirical indicators of ocean chemistry and precipitation rate: Geochimica et Cosmochimica Acta, v. 56, p. 1837-1849.

Carpenter, S.J., and Lohmann, K.C., 1997, Carbon isotope ratios of Phanerozoic marine cements: Re-evaluating the global carbon and sulfur systems: Geochimica et Cosmochimica Acta, v. 61, p. 4831-4846.

Cicero, A.D., and Lohmann, K.C., 2001, Sr/Mg variation during rock-water interaction: Implications for secular changes in the elemental chemistry of ancient seawater: Geochimica et Cosmochimica Acta, v. 65, p. 741-761.

Crawford, G. A., 1989, Goat Seep – Precursor to the Capitan, in, Harris, P. M., and Grover, G. A., Subsurface and outcrop examination of the Capitan shelf margin, northern Delaware Basin, SEPM Core Workshop no. 13, p. 373-378.

Crysdale, B.L., 1987, Fluid inclusion evidence for the origin, diagenesis, and thermal history of sparry calcite cement in the Capitan Limestone, McKittrick Canyon, W. Texas: University of Northern Colorado, Master's thesis, 68 p.

Cys, J. M., Toomey, D. F., Brezina, J. L., Greenwood, E., Groves, D. B., Klement, K. W., Kullmann, J. D., McMillan, T. L., Schmidt, V., Sneed, E. D., Wagner, L. H., 1977, Capitan Reef – Evolution of a Concept, in, Hileman, M. E., and Mazzullo, S. J. (eds.), Upper Guadalupian facies, Permian Reef Complex, Guadalupe Mountains, New Mexico and West Texas: 1977 Field Conference Guidebook, Permian Basin Section, SEPM Publication 77-16, p. 201-322.

Dickson, J.A.D., 2002, Echinoderm skeletal preservation: Calcite/aragonite seas and the Mg/Ca ratio of Phanerozoic oceans: Science, v. 298, p. 1222-1224.

Dickson, J.A.D., 2004, Echinoderm skeletal preservation: Calcite-Aragonite seas and the Mg/Ca ratio of Phanerozoic oceans: Journal of Sedimentary Research, v. 74, p. 355-365.

Garber, R. A., and Grover, G. A., 1989, Geology of the Capitan shelf margin – Subsurface data from the northern Delaware Basin, in, Harris, P. M., and Grover, G. A., Subsurface and outcrop examination of the Capitan shelf margin, northern Delaware Basin, SEPM Core Workshop no. 13, p. 3-268.

Given and Lohmann, 1985, Derivation of the original isotopic composition of Permian marine cements: Journal of Sedimentary Petrology, v. 55, p. 430-439.

Given and Lohmann, 1986, Isotopic evidence for the early meteoric diagenesis of the reef facies, Permian Reef Complex of West Texas and New Mexico: Journal of Sedimentary Petrology, v. 56, p. 183-193.

Glover, E.D., 1961, Method of solution of calcareous materials using the complexing agent, EDTA: Journal of sedimentary petrology, v. 31, p. 622-626.

Hardie, L.A., 1996, Secular variation in seawater chemistry: An explanation for the coupled secular variations in the mineralogies of marine limestones and potash evaporates over the past 600 m.y.: Geology, v. 24, p. 279-283.

Hartley, G., and Mucci, A., 1996, The influence of P_{CO2} on the partitioning of magnesium calcite overgrowths precipitated from artificial seawater at 25° and 1 atm total pressure: Geochimica et Cosmochimica Acta, v. 60, p. 315-324.

Hasiuk, F.J., 2005, Mississippian ocean chemistry inferred from biotic and abiotic carbonate phases at Muleshoe Mound, Lake Valley Formation, Alamagordo, New Mexico: University of Michigan, Master's Thesis.

Hill, C. A., 1996, Geology of the Delaware Basin, Guadalupe, Apache, and Glass Mountains, New Mexico and West Texas: Permian Basin Section, SEPM, Publication no. 96-39, 480 p.

Hills, J. M., 1984, The structural evolution of the Permian Basin of West Texas and New Mexico, in, The Geologic Evolution of the Permian Basin, A Symposium, Permian Basin Section SEPM, Program with Abstracts, p. 8-9.

Holland, H.D., and Zimmermann, H., 2000, The dolomite problem revisited: International Geologic Review, v. 12, p. 481-490.

Horita, J., Friedman, T.J., Lazar, B., and Holland, H.D., 1991, The composition of Permian seawater: Geochimica et Cosmochimica Acta, v. 55, p. 417-432

Horita, J., Zimmermann, H., and Holland, H.D., 2002, Chemical evolution of seawater during the Phanerozoic: Implications from the record of marine evaporites: Geochimica et Cosmochimica Acta, v. 66, p. 3733-3756.

Katz, A., 1973, The interaction of magnesium with calcite during crystal growth at 25-90°C and one atmosphere: Geochimica et Cosmochimica Acta, v. 37, p. 1563-1586.

Kendall, C. G. ST. C., 1969, An environmental re-interpretation of the Permian evaporate/carbonate shelf sediments of the Guadalupe Mountains: Geological Society of America Bulletin, v. 80, p. 2503-2526.

Kirkland, B. L., and Chapman, R. L., 1990, The fossil green alga *Mizzia* (Dasycladaceae): A tool for interpretation of paleoenvironment in the Upper Permian Capitan Reef Complex, Southeastern New Mexico: Journal of Phycology, v. 26, p. 569-576.

Kirkland-George, B., 1992, Distinctions between reefs and bioherms based on studies of fossil algae: *Mizzia*, Permian Reef Complex (Guadalupe Mountains, Texas and New Mexico, and *Eugonophyllum*, Pennsylvanian Holder Formation (Sacramento Mountains, New Mexico: Applied Carbonate Research Program Technical Series Contribution #67, Modified from Ph.D. dissertation, Louisiana State University, 156 p.

Kluth, C. F., and Coney, P. J., 1981, Plate tectonics of the Ancestral Rocky Mountains: Geology, v. 9, p. 10-15.

Lloyd, E. R., 1929, Capitan Limestone and associated formation of New Mexico and Texas: American Association of Petroleum Geologists Bulletin, v. 13, p. 645-658.

Lohmann and Meyers, 1977, Microdolomite inclusions in cloudy prismatic calcites; a proposed criterion for former high-magnesium calcites: Journal of Sedimentary Petrology, v. 47, p. 1078-1088.

Lowenstein, T.K., Hardie, L.A., Timofeeff, M.N., and Demicco, R.V., 2003, Secular variation in seawater chemistry and the origin of calcium chloride basinal brines: Geology, v. 31, p. 857-860.

Lowenstein, T.K., Timofeeff, M.N., Brennan, S.T., Hardie, L.A., Demicco, R.V., 2001. Oscillations in Phanerozoic seawater chemistry: Evidence from fluid inclusions: Science 294, 1086-1088.

Major, R.P., Wilber, R.J., 1991, Crystal habit, geochemistry, and cathodoluminescence of magnesian calcite marine cements from the lower slope of Little Bahama Bank: Geological Society of America Bulletin, v. 103, p. 461-471.

Mazzullo, S. J., and Cys, J. M., 1977, Submarine cements in Permian boundstones and reef-associated rocks, Guadalupe Mountains, West Texas and Southeastern New Mexico, in, Hileman, M. E., and Mazzullo, S. J. (eds.), Upper Guadalupian facies, Permian Reef Complex, Guadalupe Mountains, New Mexico and West Texas: 1977 Field Conference Guidebook, Permian Basin Section, SEPM Publication 77-16, p. 151-200.

McKnight, C. L., 1984, Structural Evolution of the Guadalupe Mountains Region, Southeastern New Mexico and West Texas, in, The Geologic Evolution of the Permian Basin, A Symposium, Permian Basin Section SEPM, Program with Abstracts, p. 27-28.

Melim and Scholle, 1989, Dolomitization model for the forereef facies of the Permian Capitan Formation, Guadalupe Mountains, Texas – New Mexico, in, Harris, P. M., and Grover, G. A., Subsurface and outcrop examination of the Capitan shelf margin, northern Delaware Basin, SEPM Core Workshop no. 13, p. 407-413.

Mruk, D. H., 1985, Cementation and dolomitization of the Capitan Limestone (Permian) McKittrick Canyon, West Texas: University of Colorado, Master's thesis, 155 p.

Mucci, A., 1987, Influence of temperature on the composition of magnesium calcite overgrowths precipitated from seawater: Geochimica et Cosmochimica Acta, v. 51, p. 1977-1984.

Mucci, A., Canuel, R., and Zhong, S., 1989, The solubility of calcite and aragonite in sulfate-free seawater and the seeded growth kinetics and composition of the precipitates at 25°C: Chemical Geology, v. 74, p. 309-320.

Mucci, A., and Morse, J.W., 1983, The incorporation of Mg2+ and Sr2+ into calcite overgrowths: influence of growth rate and solution composition: Geochimica et Cosmochimica Acta, v. 47, p. 217-233.

Rahnis, M. A., and Kirkland, B. L., 1999, Distribution, petrography, and geochemical characterization of radiaxial calcite and associated diagenetic events in the Capitan Formation, West Texas and New Mexico, in, Saller, A. H., Harris, P. M., Kirkland, B. L., and Mazzullo, S. J. (eds.), Geologic Framework of the Capitan Reef: SEPM Special Publication no. 65, p. 175-191.

Ries, J.B., 2004, Effect of ambient Mg/Ca ratio of Mg fractionation in calcareous marine invertebrates: A record of the oceanic Mg/Ca ratio over the Phanerozoic: Geology, v. 32, p. 981-984.

Sandberg, P.A., 1983, An oscillating trend in Phanerozoic nonskeletal carbonate mineralogy: Nature, v. 305, p. 19-22.

Stanley, S.M., and Hardie, L.A. 1998. Secular oscillations in the carbonate mineralogy of reef-building and sediment-producing organisms driven by tectonically forced shifts in seawater chemistry: Palaeogeography, Palaeoclimatology, Palaeoecology 144, 3-19.

Timofeeff, M.N., Lowenstein, T.K., Brennan, S.T., Demicco, R.V., Zimmermann, H., Horita, J., amd Borstel, L.E., 2001, Evaluating seawater chemistry from fluid inclusions in halite: Examples from modern marine and nonmarine environments: Geochimica et Cosmochimia Acta, v. 65, p. 2293-2300.

Videtich, P.E., 1985, Electron microprobe study of Mg distribution in recent Mg calcites and recrystallized equivalents from the Pleistocene and Tertiary: Journal of Sedimentary Petrology, v. 55, p. 421-429.

Weidlich, O., and Fagerstrom, J.A., 1999, Influence of sea-level changes on development, community structure, and quantitative composition of the upper Capitan massive (Permian), Guadalupe Mountains, Texas and New Mexico, in, Saller, A. H., Harris, P. M., Kirkland, B. L., and Mazzullo, S. J. (eds.), Geologic Framework of the Capitan Reef: SEPM Special Publication no. 65, p. 139-160.

Wilkinson, B.H., and Algeo, T.J., 1989, Sedimentary carbonate record of calcium-magnesium cycling: American Journal of Science, v. 289, p. 1158-1194.

Wilson, P.A., and Dickson, J.A.D., 1996, Radiaxial calcite: Alteration product and petrographic proxy for magnesian calcite cement: Geology, v. 24, p. 945-948.

Ye, H., Royden, L., Burchfiel, C., Schuepbach, M., 1996, Late Paleozoic Deformation of Interior North America: The Greater Ancestral Rocky Mountains: American Association of Petroleum Geologists Bulletin, v. 80, p. 1397-1432.

Yurewicz, D. A., 1977, The origin of the massive facies of the lower and middle Capitan Limestone (Permian), Guadalupe Mountains, New Mexico and West Texas, in, Hileman, M. E., and Mazzullo, S. J. (eds.), Upper Guadalupian facies, Permian Reef Complex, Guadalupe Mountains, New Mexico and West Texas: 1977 Field Conference Guidebook, Permian Basin Section, SEPM Publication 77-16, p. 45-92.
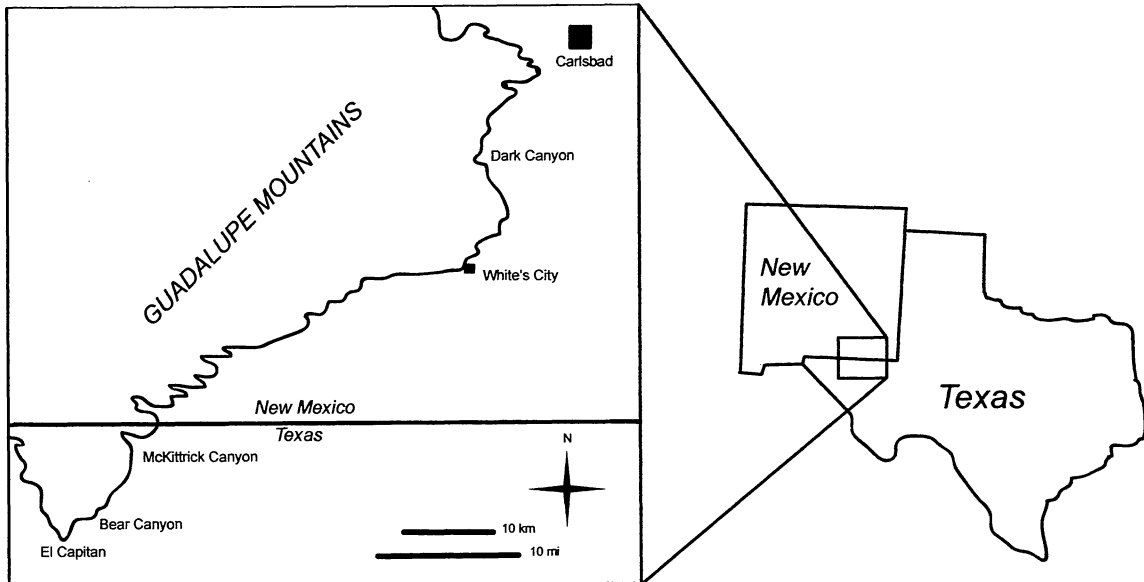
Fig. 1. Map of the Guadalupe Mountains of New Mexico and West Texas. The Permian Reef Complex follows a northeast/southwest trend and is cut by numerous canyons. Samples were collected from Bear Canyon and McKittrick Canyon.
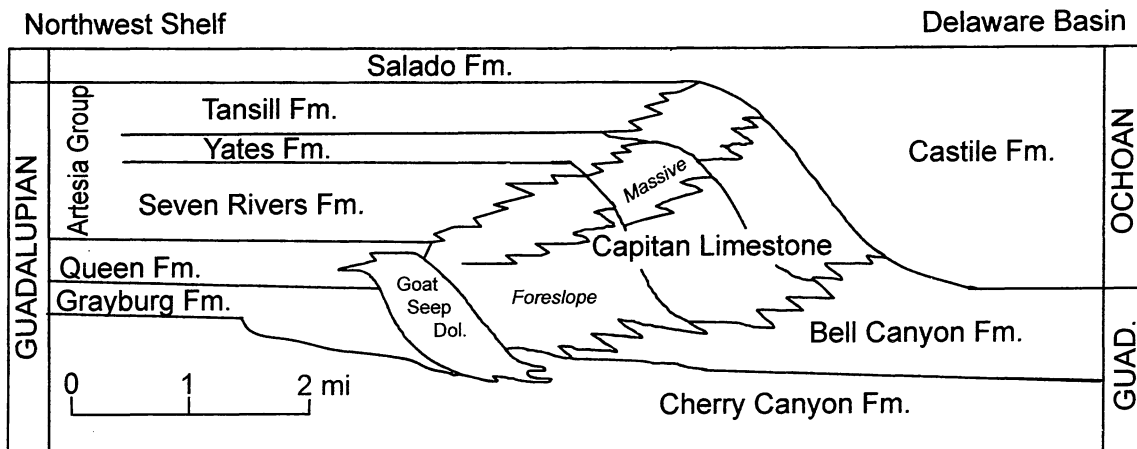
Fig. 2. Cross section of the Permian Reef Complex showing the shelf formations, the massive reef and forereef facies, and the basinal formations. Samples were collected from the massive facies of the Capitan Limestone. Samples from Bear Canyon are older and equivalent in age to the Seven Rivers Formation. Samples from McKittrick Canyon are younger and equivalent to a late Yates or early Tansill Formation age.
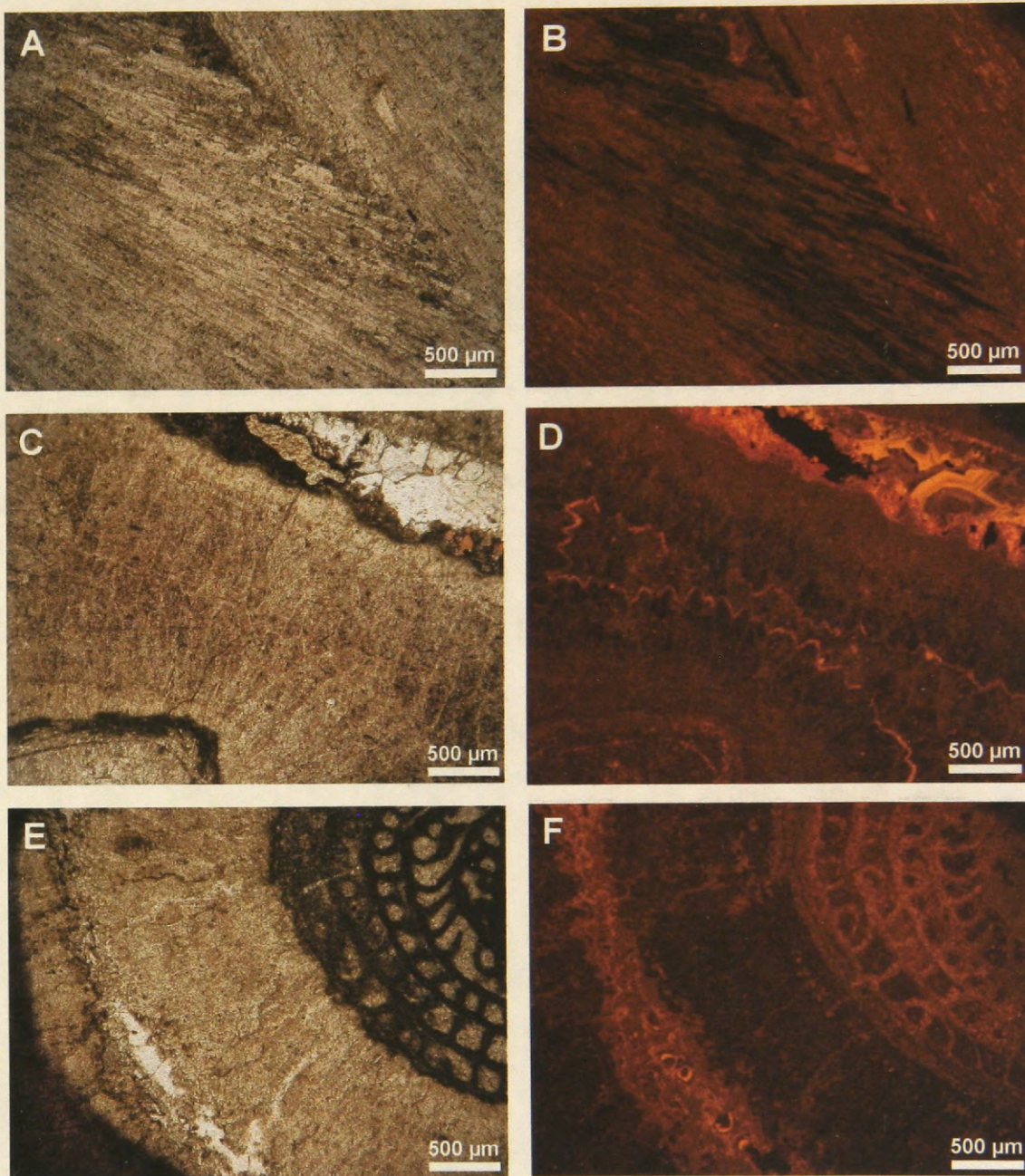
Fig. 3. Paired images. A, C, and E are polarizing light microscopy images shown with uncrossed polars. B, D, and F are cathodoluminescent microscopy images. A consists of former aragonite, and B shows nonluminescent and luminescent areas under cathodoluminescence. C and D are former magnesian calcite cement from a neptunian dike in McKittrick Canyon. E and F represent former magnesian calcite cement coating a fusilinid.
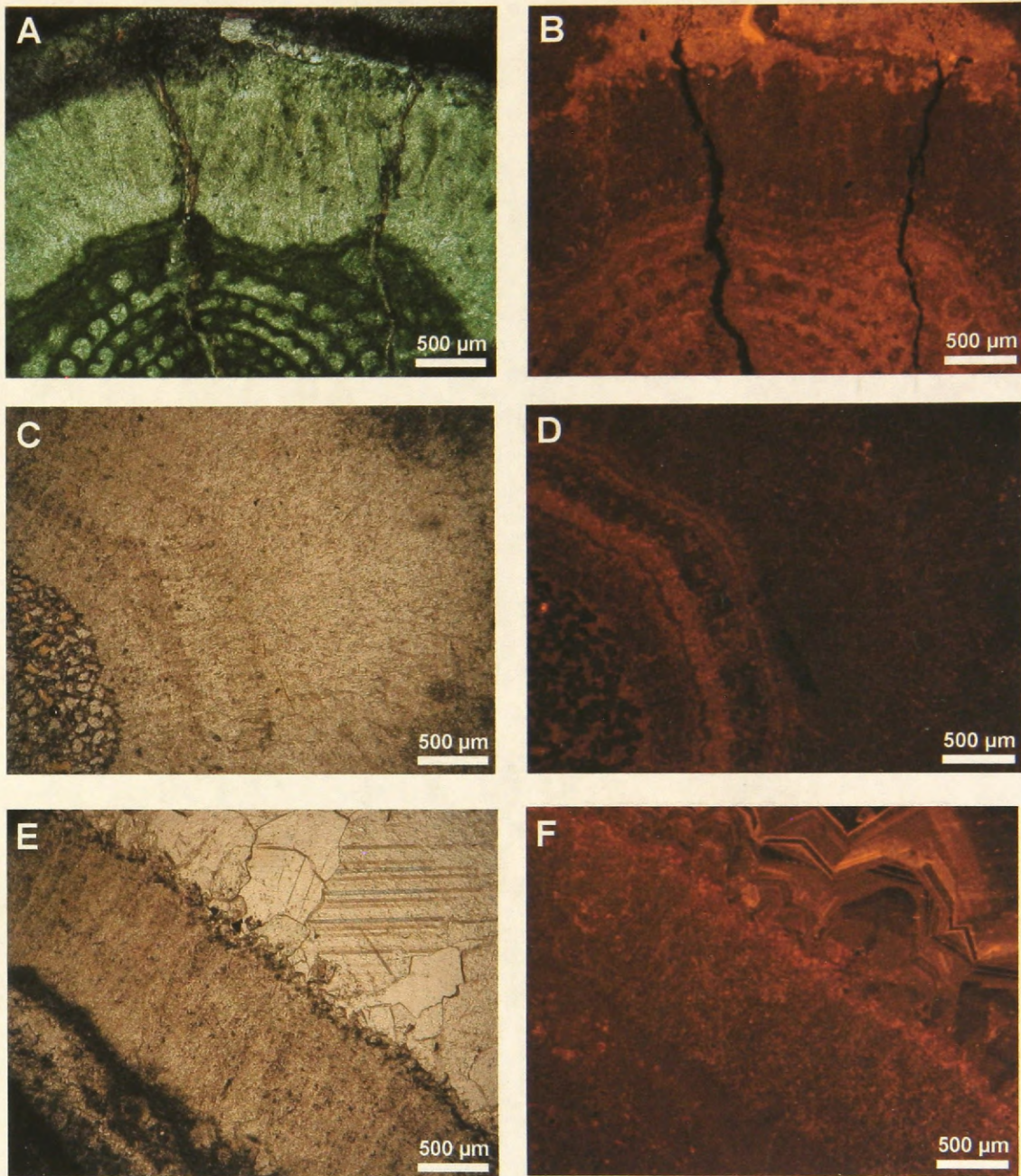
Fig. 4. Paired images former magnesian cement under polarizing light microscopy with uncrossed polars (A, C, E) and cathodoluminescent microscopy (B, D, F). Note the visible twinning planes on A. Image D shows an alternation of dull and brightly luminescent banding of the isopachous cement. Image F shows a patchy intergrowth of dull and brightly luminescent crystals with secondary reddish dolomite on the outer edge of the marine cement, and growth of brightly banded equant sparry calcite towards the outer edge.
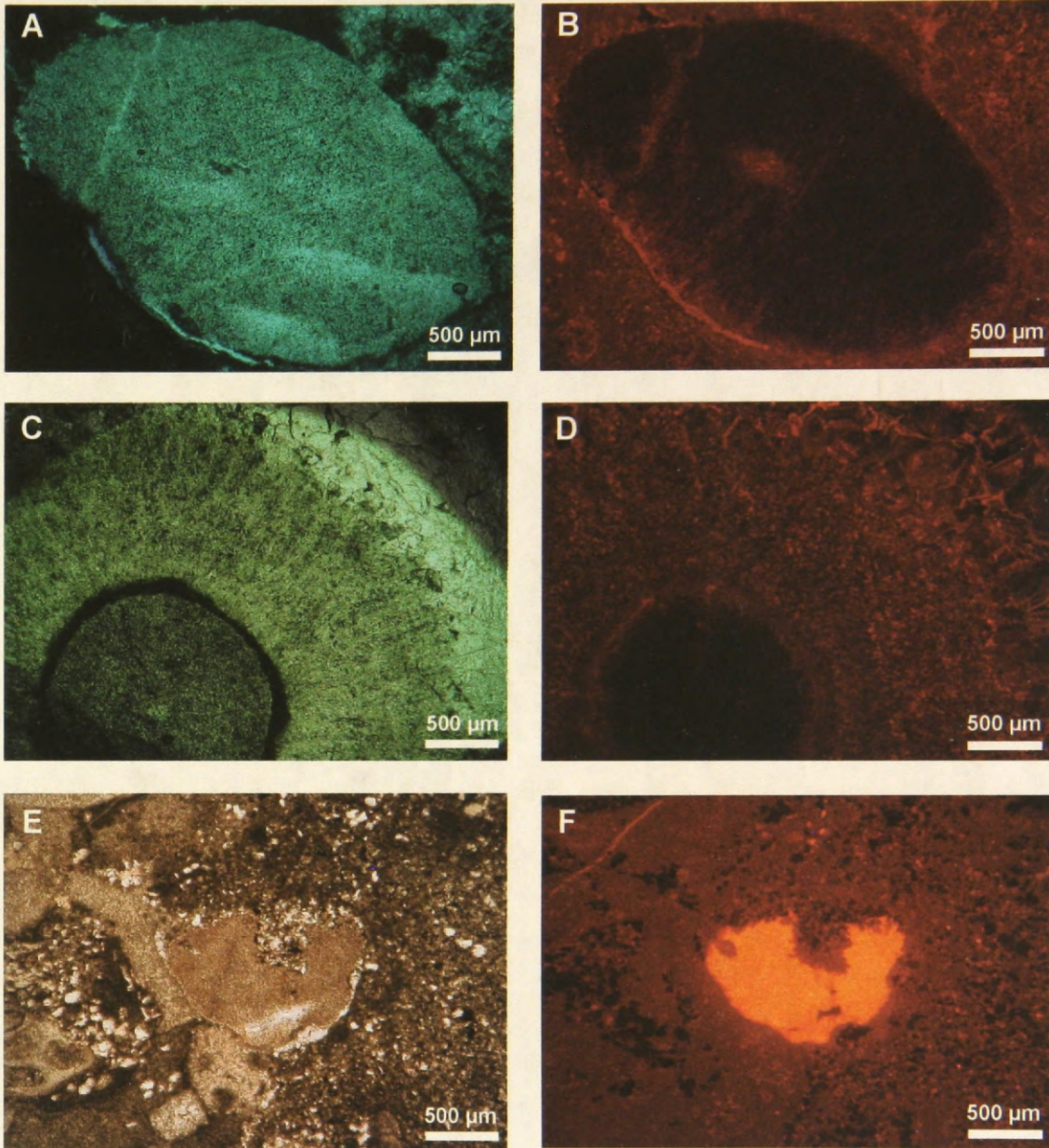
Fig. 5. Paired images crinoid fragments under polarizing light microscopy with uncrossed polars (A, C, E) and cathodoluminescent microscopy (B, D, F). Image B shows a mostly nonluminescent crinoid, C and D show a nonluminescent crinoid surrounded by a patchy dull/brightly luminescent former magnesian calcite cement. F shows a brightly luminescent crinoid.
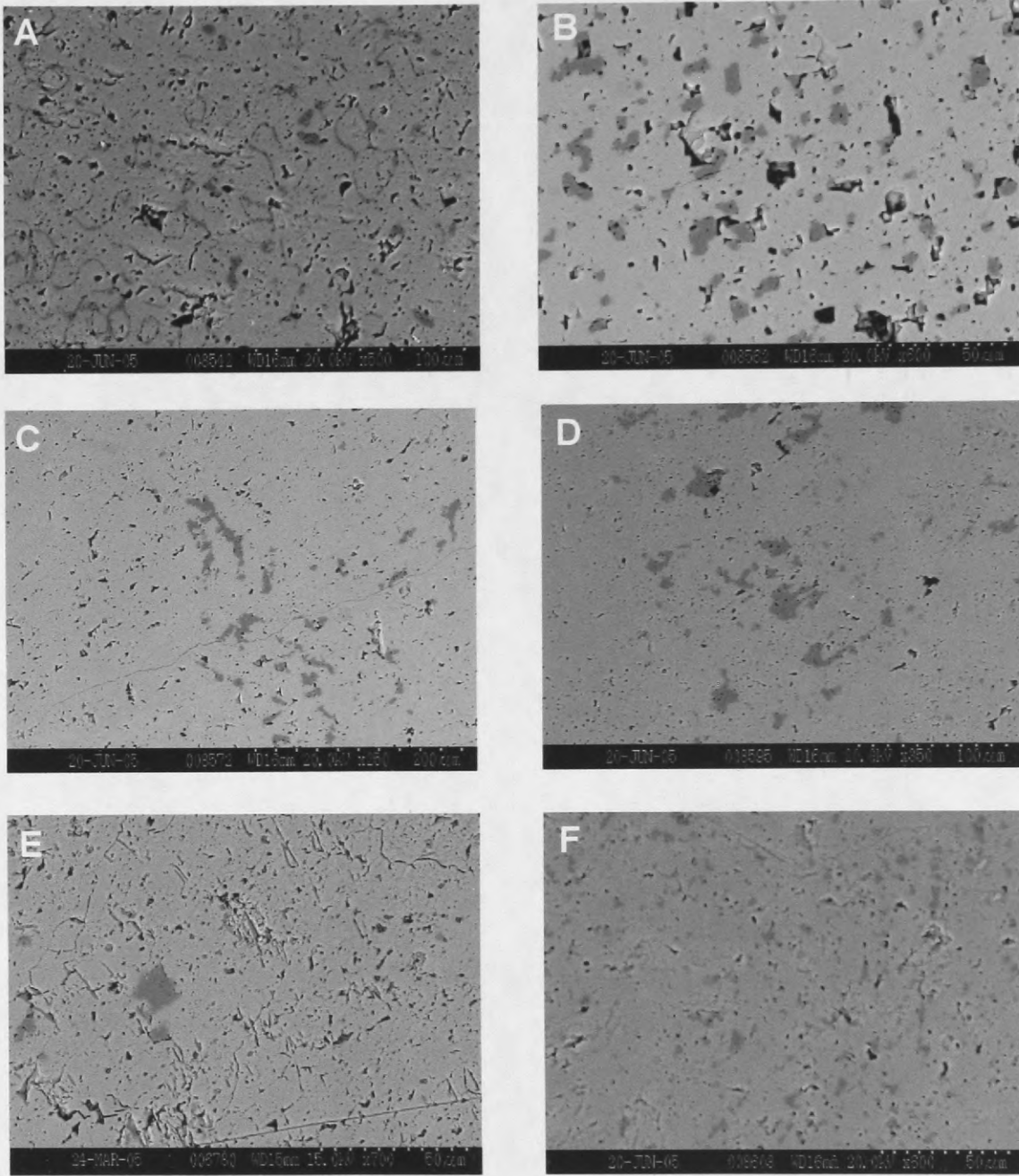
Fig. 6. SEM backscatter electron images. Calcite shows up as light gray and dolomite dark gray. A - Crinoid fragment showing remnants of stereom structure. B – Crinoid fragment showing euhedral microdolomite inclusions. C and D – Bands of subhedral to anhedral microdolomite inclusions in former magnesian calcite cements. E – A euhedral microdolomite inclusion in former magnesian calcite cement. F – Numerous microdolomite inclusions in a former magnesian calcite cement from a neptunian dike.
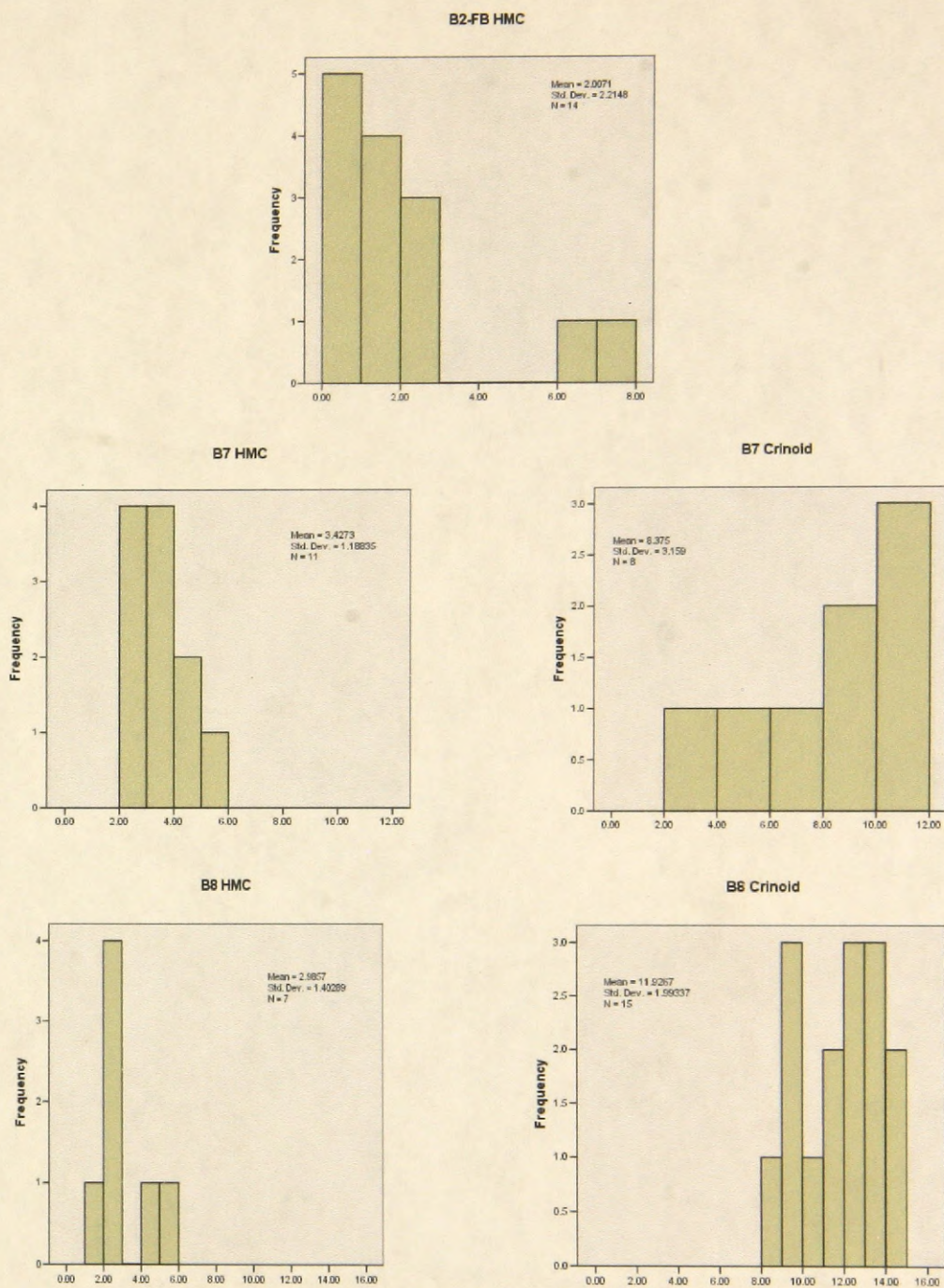
Fig. 7A. Histograms showing volumes of microdolomite in former magnesian calcite cements and crinoids from Bear Canyon. Volumes were estimated from SEM BSE images using a computer imaging system. Note that the crinoids show a higher mean percentage of microdolomite inclusions than the former HMC cements.
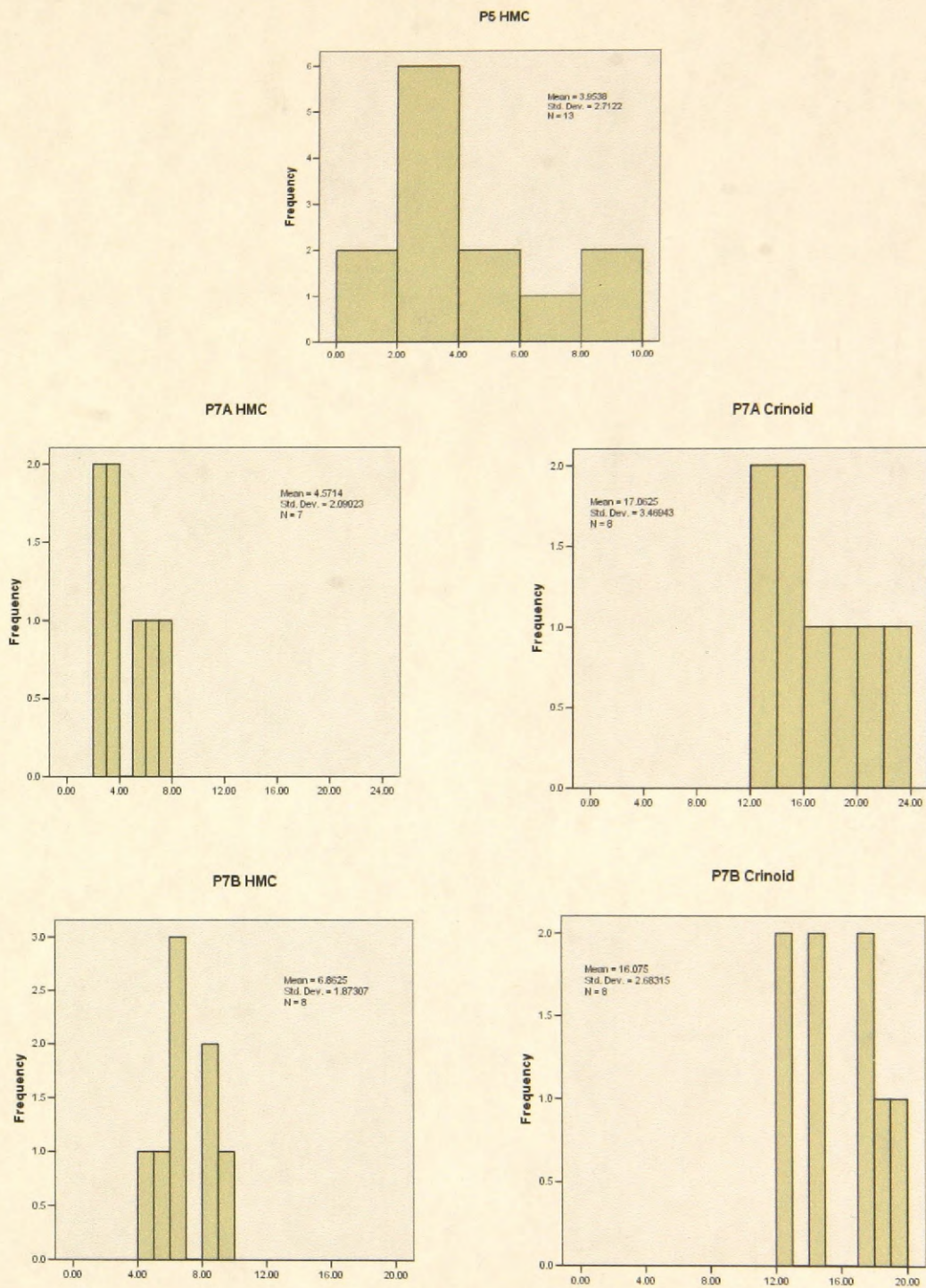
Fig. 7B. Histograms showing volumes of microdolomite in former magnesian calcite cements and crinoids from McKittrick Canyon.

Mole % MgCO3 of Microdolomites in HMC and Crinoids

Mean = 45.8373
Std. Dev. = 4.56136
N = 45
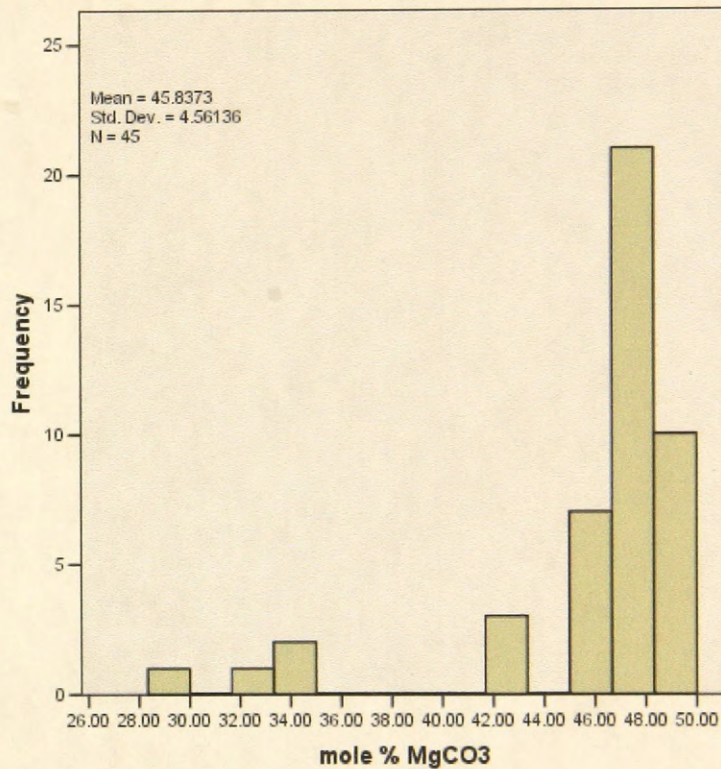
Fig. 8. Mole % $MgCO_3$ in microdolomites within former HMC cements and crinoids obtained using a microprobe. A mole % $MgCO_3$ of 48% occurs with highest frequency, indicating a dolomitic composition for the inclusions. Data from less than 40 mole % $MgCO_3$ are indicative of a small amount of calcite mixing in with a microdolomite inclusion upon analysis.
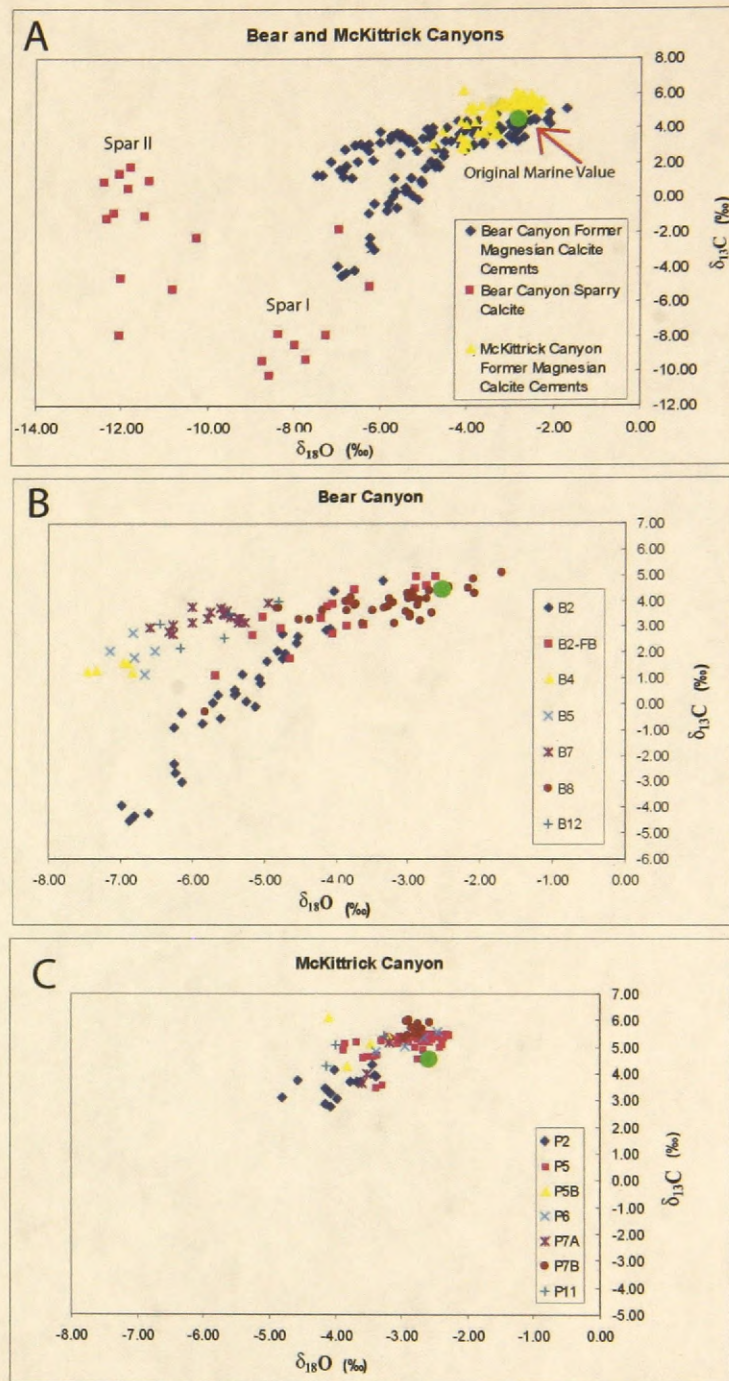
Fig. 9. Stable carbon and oxygen isotope plots. A – Former magnesian calcite cement data from Bear and McKittrick Canyons, and selected calcite spar data from Bear Canyon. The original Permian seawater value is shown in green on all plots. B – Bear Canyon former magnesian calcite cement data separated out by sample ID. Note the two covariant trends which extend back towards the Permian marine value. C – Former magnesian calcite cement data from McKittrick Canyon.
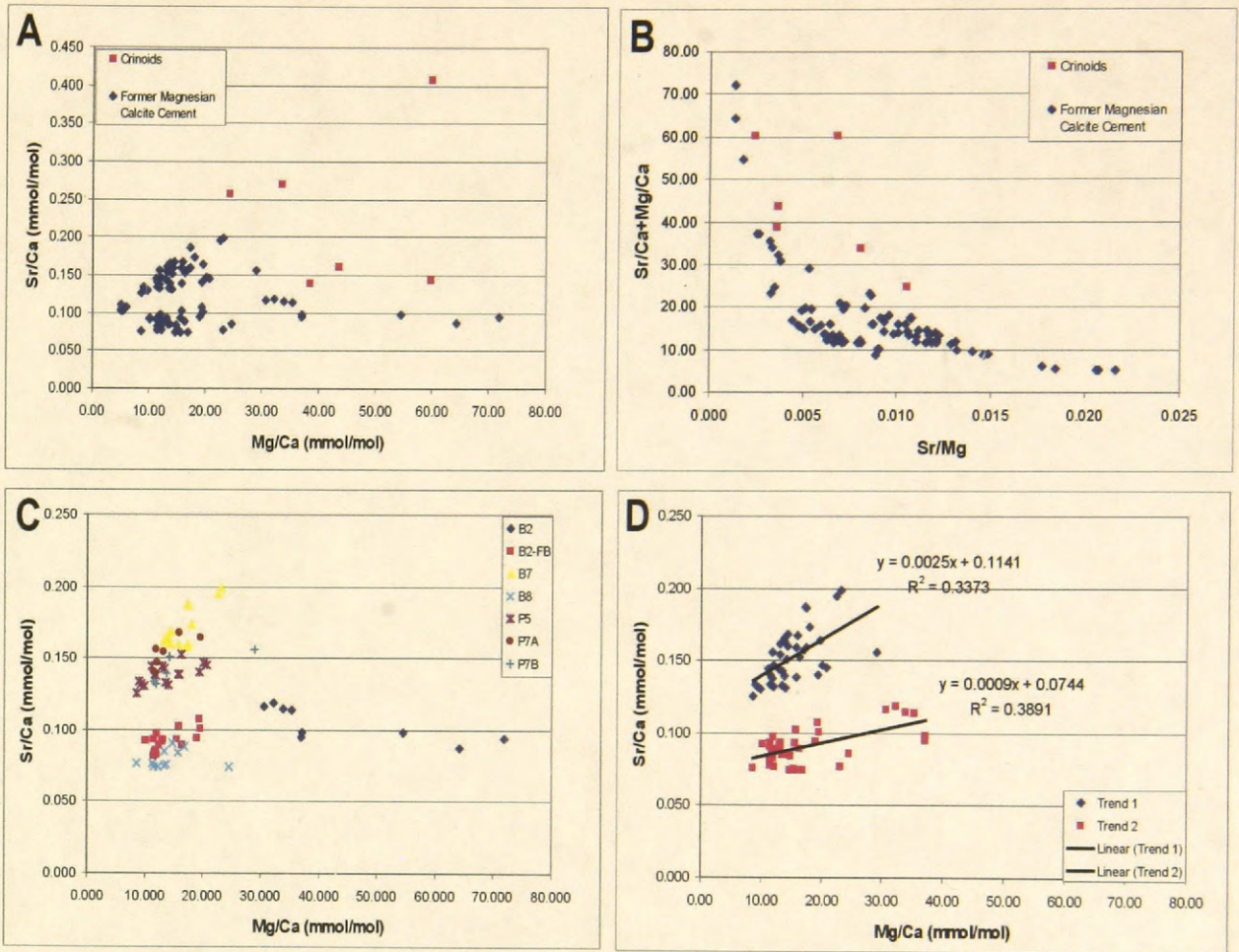
Fig. 10. A and B - Former magnesian calcite and crinoid Sr and Mg data.
C - Sr and Mg data separated out by sample. Note that the "top" clustering of data
with higher Sr amounts occur in samples from mostly McKittrick Canyon, except for
one sample from Bear Canyon. The bottom clustering of data are only from Bear
Canyon. D – Linear regression lines obtained from the two separated clusters of
data.
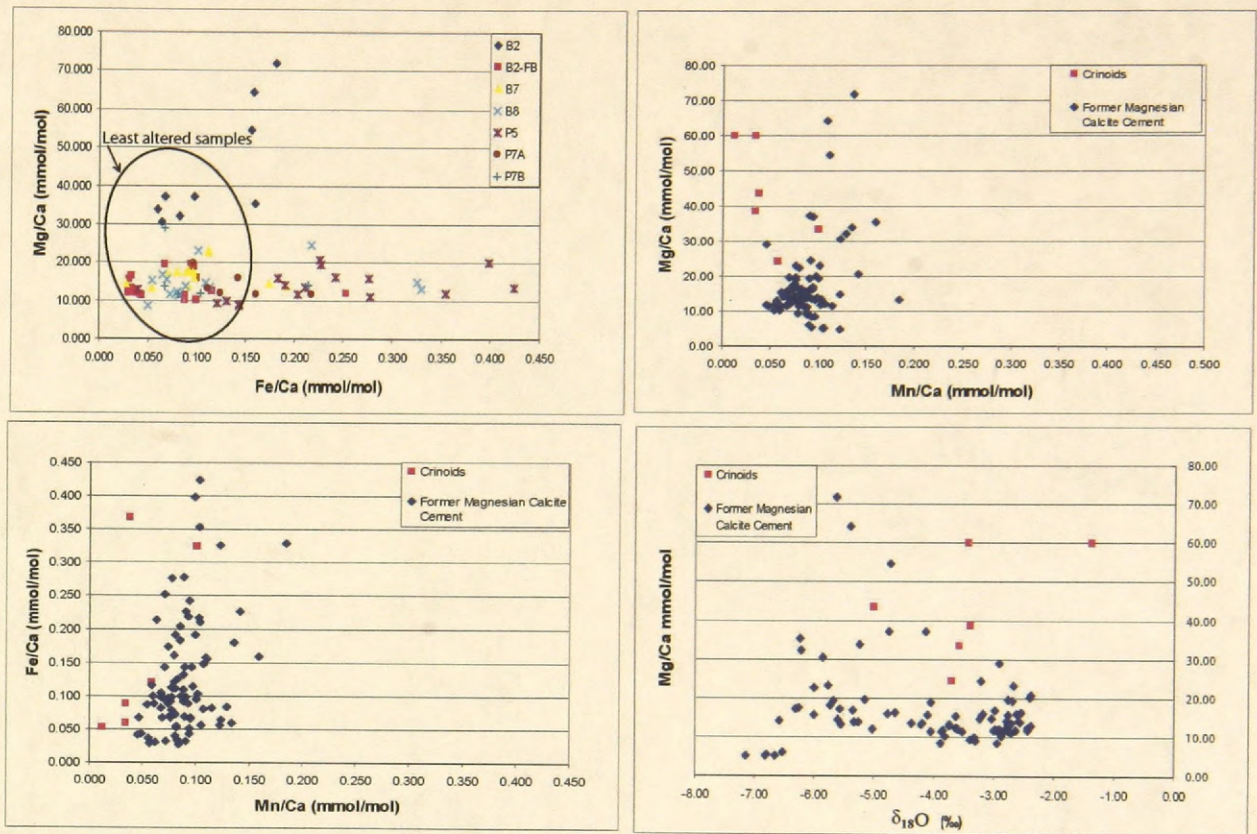
Fig. 11. Iron, manganese, magnesium and oxygen isotope data for former magnesian calcite cements and crinoids. Note that a grouping of least altered samples was defined by those samples having a Fe content less than 0.150 mmol/mol.

Sample	Type	# Analyses	Avg Mg/Ca	Mg/Ca SD	Avg Mg mol%	Mg/Ca SW	Modified Mg/Ca SW
B2	HMC cement	5	34.20	2.90	3.31	1.49	2.97
B2-FB	HMC cement	16	13.99	3.23	1.38	0.61	1.22
B7	HMC cement	11	17.26	3.19	1.70	0.75	1.50
B7	Crinoid	1	24.36	-	2.34	1.06	1.06
B8	HMC cement	11	14.25	3.77	1.40	0.62	1.24
B8	Crinoid	2	49.26	15.11	4.68	2.14	2.14
P5	HMC cement	5	9.96	1.76	0.99	0.43	0.87
P7A	HMC cement	5	14.53	3.30	1.43	0.63	1.26
P7A	Crinoid	1	59.93	-	5.65	2.61	2.61
P7B	HMC cement	4	16.56	8.33	1.62	0.72	1.44

Table 1. Calculation of a Permian Mg/Ca ratio using samples with a Fe/Ca less than 0.150 mmol/mol. An initial Mg/Ca of seawater was calculated using a D_{Mg} of 0.023, and a modified Mg/Ca of seawater was created assuming that 50% of former magnesian calcite cements are now occupied by a later luminescent diagenetic phase.
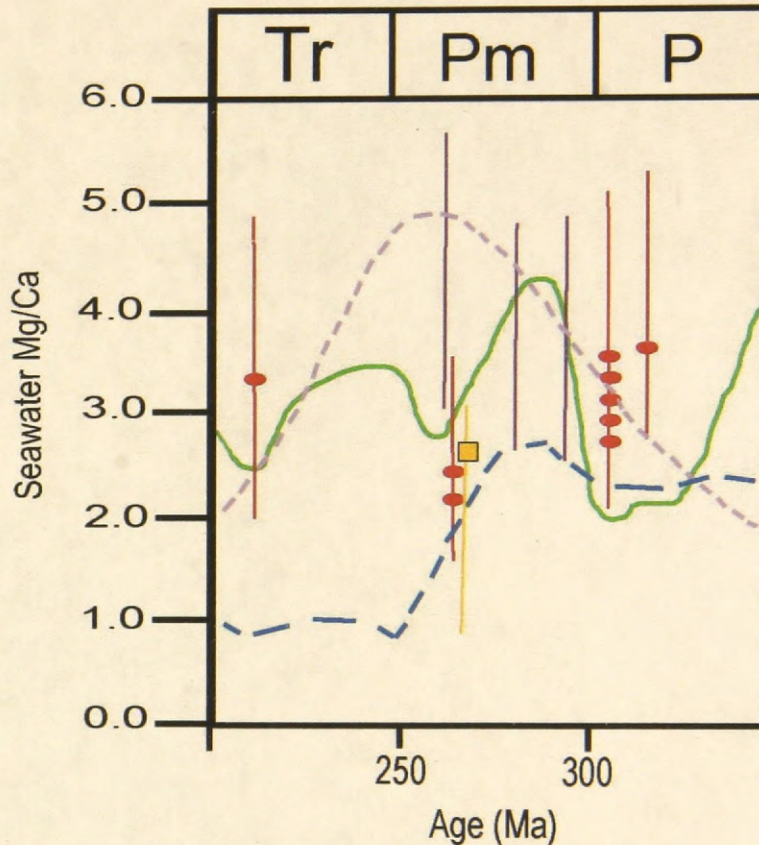
Fig. 12. Seawater Mg/Ca molar ratio versus age for the Pennsylvanian, Permian, and Triassic during a time of proposed "aragonite sea" conditions. The range for the Permian Reef former magnesian calcite cement data is shown as an orange bar, with the square representing the "most likely" value for the Mg/Ca ratio. Echinoderm data from Dickson (2004) is shown in red. The solid green line is the Mg/Ca ratio modeled by Hardie (1996) and the dashed blue line is the Mg/Ca ratio modeled by Wilkinson and Algeo (1989). The purple vertical bars plot a range of possible Mg/Ca ratios from fluid inclusion data (Lowenstein et al., 2001), and the dotted purple line is the Mg/Ca ratio estimated by fluid inclusion data from Horita et al. (2002).

APPENDIX 1

Sample ID	Location	Region	East	North	Elevation (ft)
B2	Bear Canyon	13R	516590	3531188	7501
B2-FA	Bear Canyon	13R	516590	3531188	7501
B4	Bear Canyon	13R	516587	3531248	7565
B6	Bear Canyon	13R	516534	3531344	7813
B7	Bear Canyon	13R	516449	3531351	7890
B8	Bear Canyon	13R	515398	3532063	7889
B11	Bear Canyon	13R	516476	3532431	7999
B12	Bear Canyon	13R	516553	3531282	7697
P2	McKittrick Canyon	13R	522889	3539456	5849
P5B	McKittrick Canyon	13R	522867	3539761	6239
P6	McKittrick Canyon	13R	522887	3539848	6329
P7A	McKittrick Canyon	13R	522785	3539903	6511
P7B	McKittrick Canyon	13R	522785	3539903	6511
P11	McKittrick Canyon	13R	522811	3540006	6557

APPENDIX 2

Sample Type	Sample	ID	Mineralogy	δ18O	δ13C	Mg/Ca	Mg mol%	Sr/Ca	Mn/Ca	Fe/Ca
Bulk Samples	B2	.01	Mg Calcite	-3.34	4.79					
Run 1	B2	.02	Mg Calcite	-4.03	4.38					
	B2	.03	Mg Calcite	-4.08	2.90					
	B2	.04	Mg Calcite	-4.71	1.97					
	B2	.05	Mg Calcite	-4.54	2.63					
	B4	.01	Mg Calcite	-6.96	1.60					
	B4	.02	Mg Calcite	-6.90	1.55					
	B4	.03	Mg Calcite	-6.84	1.19					
	B4	.04	Mg Calcite	-7.34	1.32					
	B4	.05	Mg Calcite	-7.47	1.26					
	B7	.01	Mg Calcite	-4.93	3.91					
	B7	.02	Mg Calcite	-5.51	3.63					
	B7	.03	Mg Calcite	-6.27	2.72					
	B7	.04	Mg Calcite	-5.46	3.36					
	B7	.05	Mg Calcite	-5.34	3.16					
	B8	.01	Mg Calcite	-4.52	3.27					
	B8	.02	Mg Calcite	-2.74	4.07					
	B8	.04	Mg Calcite	-3.27	3.80					
	B8	.05	Mg Calcite	-2.98	3.48					
	B12	.01	Mg Calcite	-6.15	2.16					
	B12	.02	Mg Calcite	-5.48	3.52					
	B12	.03	Mg Calcite	-4.79	3.99					
	B12	.04	Mg Calcite	-6.45	3.11					
	B12	.05	Mg Calcite	-5.54	2.55					
	P2	.01	Mg Calcite	-4.79	3.11					
	P2	.02	Mg Calcite	-4.56	3.77					
	P2	.03	Mg Calcite	-4.00	4.14					
	P2	.04	Mg Calcite	-4.14	2.85					
	P5B	.01	Mg Calcite	-3.18	5.39					
	P5B	.02	Mg Calcite	-3.47	5.11					
	P5B	.03	Mg Calcite	-3.82	4.30					
	P5B	.06	Mg Calcite	-4.10	6.12					
	P5	.01	Mg Calcite	-2.40	5.36					
	P5	.02	Mg Calcite	-2.47	5.44					
	P5	.03	Mg Calcite	-2.90	5.23					
	P6	.01	Mg Calcite	-2.45	5.56					
	P6	.02	Mg Calcite	-2.94	5.05					
	P6	.04	Mg Calcite	-2.68	5.37					
	P6	.05	Mg Calcite	-3.38	4.83					
	P7B	.01	Mg Calcite	-2.92	5.99					
	P7B	.02	Mg Calcite	-2.88	6.02					
	P7B	.03	Mg Calcite	-2.75	5.89					
	P7B	.04	Mg Calcite	-2.75	5.48					

	P7B	.05	Mg Calcite	-2.68	5.66
	P11	.01	Mg Calcite	-3.98	5.11
	P11	.02	Mg Calcite	-4.13	4.31
	P11	.03	Mg Calcite	-3.25	5.45
Bulk Samples	B2.	.01	Mg Calcite	-6.13	-0.34
Run 2	B2.	.02	Mg Calcite	-5.71	0.06
	B2.	.03	Mg Calcite	-5.04	0.81
	B2.	.06	Mg Calcite	-5.12	-0.09
	B2.	.07	Mg Calcite	-4.81	2.05
	B2.	.08	Mg Calcite	-4.55	2.37
	B2.	.09	Mg Calcite	-4.96	1.66
	B2.	.10	Mg Calcite	-5.06	0.99
	B2.	.11	Mg Calcite	-5.38	0.41
	B2.	.12	Mg Calcite	-5.40	0.34
	B2.	.13	Mg Calcite	-5.61	-0.56
	B2.	.14	Mg Calcite	-6.25	-0.90
	B2.	.15	Mg Calcite	-6.99	-3.96
	B2.	.16	Mg Calcite	-6.79	-4.32
	B2.	.17	Mg Calcite	-6.88	-4.51
	B2.	.18	Mg Calcite	-5.30	1.16
	B2.	.19	Mg Calcite	-6.14	-3.02
	B2.	.20	Mg Calcite	-6.61	-4.22
	B8(1).	.01	Mg Calcite	-3.01	4.29
	B8(1).	.02	Mg Calcite	-2.98	4.12
	B8(1).	.03	Mg Calcite	-2.83	3.22
	B8(1).	.04	Mg Calcite	-2.55	4.40
	B8(1).	.05	Mg Calcite	-2.85	4.04
	B8(1).	.06	Mg Calcite	-2.16	4.48
	B8(1).	.07	Mg Calcite	-2.71	4.36
	B8(2).	.01	Mg Calcite	-2.99	4.08
	B8(2).	.02	Mg Calcite	-3.49	3.65
	B8(2).	.03	Mg Calcite	-3.84	3.65
	B8(2).	.04	Mg Calcite	-2.09	4.86
	B8(2).	.05	Mg Calcite	-2.85	3.81
	B8(2).	.06	Mg Calcite	-4.80	3.73
	B8(2).	.06	Mg Calcite	-4.81	3.71
	B8(3).	.01	Mg Calcite	-5.81	-0.33
	B8(3).	.02	Mg Calcite	-2.08	4.27
	B8(3).	.03	Mg Calcite	-1.69	5.09
	B8(3).	.04	Mg Calcite	-3.74	3.82
	B8(3).	.05	Mg Calcite	-3.80	4.12
	B8(3).	.06	Mg Calcite	-3.26	4.07
	B8(3).	.07	Mg Calcite	-2.43	4.50
Bulk Samples	P2	.01	Mg Calcite	-3.97	3.04
Run 3	P2	.02	Mg Calcite	-3.38	3.92
	P2	.03	Mg Calcite	-3.39	3.97

	P2	.04	Mg Calcite	-3.76	3.70
	P2	.05	Mg Calcite	-3.66	3.70
	P2	.06	Mg Calcite	-3.61	3.69
	P2	.07	Mg Calcite	-3.43	4.35
	P2	.08	Mg Calcite	-4.08	2.78
	P2	.09	Mg Calcite	-4.15	3.46
	P2	.10	Mg Calcite	-4.07	3.25
	P5(2)	.01	Mg Calcite	-3.60	4.62
	P5(2)	.02	Mg Calcite	-3.55	4.69
	P5(2)	.03	Mg Calcite	-3.43	4.69
	P5(2)	.04	Mg Calcite	-3.38	4.71
	P5(2)	.05	Mg Calcite	-2.67	5.49
	P5(2)	.06	Mg Calcite	-2.75	5.47
	P5(2)	.07	Mg Calcite	-2.55	5.52
	P5(2)	.08	Mg Calcite	-2.59	5.41
	P5(2)	.09	Mg Calcite	-2.63	5.51
	P5(2)	.10	Mg Calcite	-2.68	5.52
	P5(3)	.01	Mg Calcite	-2.29	5.47
	P5(3)	.02	Mg Calcite	-2.40	5.48
	P5(3)	.03	Mg Calcite	-2.77	5.32
	P5(3)	.04	Mg Calcite	-3.07	5.17
	P5(3)	.05	Mg Calcite	-2.58	5.38
	P5(3)	.06	Mg Calcite	-2.68	5.38
	P5(3)	.07	Mg Calcite	-3.12	5.35
	P5(3)	.08	Mg Calcite	-3.08	5.26
	P5(3)	.09	Mg Calcite	-2.80	5.41
	P5(3)	.10	Mg Calcite	-2.70	5.47
	P5(4)	.01	Mg Calcite	-3.87	5.18
	P5(4)	.02	Mg Calcite	-3.22	5.40
	P5(4)	.03	Mg Calcite	-2.99	5.34
	P5(4)	.04	Mg Calcite	-2.99	5.39
	P5(4)	.05	Mg Calcite	-2.66	5.39
	P5(4)	.06	Mg Calcite	-3.18	5.38
	P5(4)	.07	Mg Calcite	-3.27	5.31
	P5(4)	.08	Mg Calcite	-3.70	5.24
	P5(4)	.09	Mg Calcite	-3.05	5.42
	P5(4)	.10	Mg Calcite	-2.32	5.54
Bulk Samples	B2-FA.	.01	Calcite Spar	-11.85	0.49
Run 4	B2-FA.	.02	Calcite Spar	-10.24	-2.34
	B2-FA.	.03	Calcite Spar	-12.17	-0.89
	B2-FA.	.04	Calcite Spar	-12.41	0.93
	B6	.01	Calcite Spar	-11.78	1.75
	B6	.02	Calcite Spar	-6.96	-1.81
	B6	.03	Calcite Spar	-12.04	1.39
	B6	.04	Calcite Spar	-11.36	0.93
	B8 (1)	.01	Calcite Spar	-6.22	-5.13
	B8 (1)	.02	Calcite Spar	-8.37	-7.85

Sample		Type		
B8 (2)	.01	Calcite Spar	-10.82	-5.27
B8 (2)	.02	Calcite Spar	-12.06	-7.94
B8 (2)	.03	Calcite Spar	-8.72	-9.41
B8 (3)	.01	Calcite Spar	-7.96	-8.47
B8 (3)	.02	Calcite Spar	-11.99	-4.63
B8 (3)	.03	Calcite Spar	-7.26	-7.98
B11	.01	Calcite Spar	-11.46	-1.05
B11	.02	Calcite Spar	-12.35	-1.23
B11	.03	Calcite Spar	-7.71	-9.37
B11	.04	Calcite Spar	-8.54	-10.31

	Sample		Type						
Micromilled Samples Run 1	B2-FB(1)	.01	Mg Calcite	-4.05	3.86	11.50	1.137	0.094	0.061	0.088
	B2-FB(1)	.02	Mg Calcite	-3.62	3.06	12.51	1.235	0.089	0.058	0.116
	B2-FB(2)	.01	Mg Calcite	-3.82	3.96	10.16	1.006	0.093	0.060	0.099
	B2-FB(2)	.02	Mg Calcite	-2.87	4.91	10.21	1.011	0.092	0.054	0.087
	B2-FB(2)	.03	Mg Calcite	-5.02	3.37	12.01	1.186	0.097	0.071	0.253
	B5(1)	.01	Mg Calcite	-6.66	1.16	5.05	0.503	0.105	0.105	0.055
	B5(1)	.02	Mg Calcite	-6.82	2.78	5.14	0.511	0.111	0.107	0.148
	B5(1)	.03	Mg Calcite	-7.15	2.08	5.00	0.497	0.103	0.122	0.056
	B5(2)	.01	Mg Calcite	-6.80	1.80	5.55	0.552	0.102	0.093	0.044
	B5(2)	.02	Mg Calcite	-6.52	2.08	6.06	0.602	0.107	0.091	0.032
	B7(1)	.01	Mg Calcite	-5.74	3.55	17.98	1.767	0.173	0.076	0.091
	B7(1)	.02	Mg Calcite	-6.32	2.83	17.35	1.705	0.187	0.075	0.097
	B7(1)	.03	Mg Calcite	-6.00	3.76	22.51	2.202	0.195	0.081	0.111
	B7(1)	.04	Crinoid	-3.70	4.64	24.36	2.378	0.258	0.058	0.121
	B7(2)	.01	Mg Calcite	-5.57	3.53	17.26	1.697	0.187	0.074	0.089
	B7(2)	.02	Mg Calcite	-5.77	3.30	23.15	2.263	0.199	0.077	0.112
	B8(1)	.01	Mg Calcite	-3.32	3.74	27.27	2.655	0.086	0.124	0.874
	B8(1)	.02	Mg Calcite	-4.19	3.60	13.44	1.326	0.085	0.097	0.113
	B8(1)	.03	Crinoid	-5.01	4.65	43.61	4.179	0.162	0.038	0.368
	B8(1)	.04	Crinoid	-3.43	5.40	59.94	5.655	0.144	0.034	0.059
	B8(3)	.01	Crinoid	-3.39	5.31	38.58	3.714	0.139	0.035	0.088
	B8(3)	.02	Mg Calcite	-3.20	3.91	24.59	2.400	0.086	0.093	0.218
	B8(3)	.03	Mg Calcite	-2.91	4.14	11.54	1.141	0.077	0.081	0.073
	B8(3)	.04	Mg Calcite	-4.36	3.25	13.72	1.354	0.085	0.093	0.089
	P5(3)	.01	Mg Calcite	-2.71	5.29	13.37	1.319	0.143	0.104	0.211
	P5(3)	.02	Mg Calcite	-2.70	5.35	11.20	1.108	0.144	0.089	0.278
	P5(3)	.03	Mg Calcite	-2.55	5.34	16.33	1.607	0.153	0.094	0.242
	P5(4)	.01	Mg Calcite	-2.38	5.21	20.73	2.031	0.145	0.142	0.226
	P5(4)	.02	Mg Calcite	-2.76	4.60	15.82	1.558	0.138	0.078	0.276
	P7A	.01	Crinoid	-1.39	5.76	59.93	5.653	0.407	0.012	0.053
	P7A	.02	Mg Calcite	-3.60	3.67	12.09	1.194	0.147	0.083	0.125
	P7A	.03	Mg Calcite	-3.00	5.39	11.83	1.169	0.156	0.102	0.217
	P7A	.04	Mg Calcite	-3.17	5.19	15.94	1.569	0.168	0.071	0.142
	P7B(1)	.01	Mg Calcite	-2.89	5.44	28.97	2.816	0.156	0.046	0.068
	P7B(1)	.02	Mg Calcite	-2.78	5.50	14.21	1.401	0.151	0.063	0.214
	P7B(1)	.03	Mg Calcite	-2.56	5.90	13.80	1.361	0.140	0.069	0.067

	Sample		Material							
	P7B(2)	.01	Crinoid	-3.58	6.07	33.44	3.235	0.270	0.100	0.325
Micromilled	B2	.02	Mg Calcite	-4.73	1.75	54.563	5.174	0.098	0.111	0.156
Samples	B2	.03	Mg Calcite	-4.13	2.89	37.155	3.582	0.098	0.091	0.098
Run 2	B2	.04	Mg Calcite	-4.74	2.74	37.053	3.573	0.095	0.095	0.068
	B2	.05	Mg Calcite	-5.40	0.55	64.295	6.041	0.087	0.109	0.157
	B2	.06	Mg Calcite	-5.65	0.34	71.934	6.710	0.094	0.136	0.180
	B2	.08	Mg Calcite	-5.24	0.09	33.941	3.282	0.115	0.134	0.060
	B2	.09	Mg Calcite	-6.22	-2.70	32.201	3.119	0.119	0.129	0.083
	B2	.10	Mg Calcite	-5.85	-0.76	30.626	2.971	0.116	0.123	0.064
	B2	.11	Mg Calcite	-6.25	-2.33	35.346	3.414	0.114	0.159	0.160
	B2-FB(1)	.01	Mg Calcite	-2.73	4.57	11.512	1.138	0.082	0.049	0.044
	B2-FB(1)	.02	Mg Calcite	-2.62	4.94	11.798	1.166	0.085	0.046	0.042
	B2-FB(1)	.03	Mg Calcite	-2.90	4.50	12.063	1.192	0.083	0.056	0.037
	B2-FB(1)	.04	Mg Calcite	-3.85	3.02	11.914	1.177	0.086	0.058	0.030
	B2-FB(1)	.05	Mg Calcite	-4.05	2.72	19.019	1.866	0.094	0.077	0.097
	B2-FB(1)	.06	Mg Calcite	-4.77	2.90	15.862	1.561	0.103	0.086	0.099
	B2-FB(1)	.07	Mg Calcite	-4.64	1.78	16.397	1.613	0.089	0.083	0.033
	B2-FB(2)	.01	Mg Calcite	-4.11	3.75	15.589	1.535	0.094	0.062	0.031
	B2-FB(2)	.02	Mg Calcite	-3.74	4.43	13.043	1.287	0.092	0.056	0.030
	B2-FB(2)	.03	Mg Calcite	-5.68	1.12	19.461	1.909	0.107	0.101	0.095
	B2-FB(2)	.04	Mg Calcite	-4.20	3.32	13.261	1.309	0.093	0.072	0.033
	B2-FB(2)	.06	Mg Calcite	-5.15	2.67	19.579	1.920	0.100	0.076	0.067
	B7(1)	.01	Mg Calcite	-6.58	2.98	14.304	1.410	0.160	0.074	0.174
	B7(1)	.02	Mg Calcite	-6.26	3.08	17.410	1.711	0.159	0.077	0.079
	B7(1)	.03	Mg Calcite	-6.00	3.18	15.781	1.553	0.160	0.068	0.097
	B7(1)	.04	Mg Calcite	-5.35	3.30	17.030	1.674	0.158	0.077	0.070
	B7(2)	.01	Mg Calcite	-5.33	3.31	13.756	1.357	0.166	0.080	0.192
	B7(2)	.02	Mg Calcite	-5.26	3.18	13.861	1.367	0.163	0.089	0.091
	B7(2)	.03	Mg Calcite	-5.60	3.72	14.412	1.420	0.168	0.084	0.027
	B7(2)	.04	Mg Calcite	-5.55	3.45	13.157	1.298	0.161	0.082	0.054
	B8(1)	.01	Mg Calcite	-3.19	3.11	15.692	1.545	0.074	0.090	0.069
	B8(1)	.02	Mg Calcite	-2.98	3.36	16.880	1.660	0.075	0.095	0.065
	B8(2)	.02	Mg Calcite	-2.94	4.35	8.586	0.851	0.076	0.093	0.051
	B8(2)	.03	Mg Calcite	-3.03	3.56	14.890	1.467	0.084	0.122	0.326
	B8(2)	.04	Mg Calcite	-3.73	3.90	13.322	1.315	0.088	0.185	0.330
	B8(2)	.05	Mg Calcite	-2.44	4.54	12.271	1.212	0.077	0.107	0.081
	B8(3)	.01	Mg Calcite	-3.86	3.97	11.404	1.127	0.091	0.115	0.082
	B8(3)	.02	Mg Calcite	-3.63	3.12	15.404	1.517	0.075	0.082	0.055
	B8(3)	.03	Mg Calcite	-3.24	3.94	14.642	1.443	0.074	0.089	0.109
	B8(3)	.04	Mg Calcite	-2.67	3.50	23.161	2.263	0.077	0.102	0.102
	P5(2)	.01	Mg Calcite	-2.38	5.36	12.999	1.283	0.144	0.080	0.039
	P5(3)	.01	Mg Calcite	-3.39	3.53	9.354	0.927	0.132	0.079	0.121
	P5(3)	.02	Mg Calcite	-3.31	3.61	9.000	0.892	0.134	0.089	0.143
	P5(3)	.03	Mg Calcite	-2.61	5.34	15.873	1.562	0.139	0.086	0.183
	P5(3)	.04	Mg Calcite	-2.69	5.24	19.450	1.908	0.140	0.091	0.227
	P5(3)	.05	Mg Calcite	-2.39	5.12	20.094	1.970	0.146	0.098	0.399
	P5(3)	.06	Mg Calcite	-2.81	5.01	11.640	1.150	0.139	0.085	0.204

P5(3)	.07	Mg Calcite	-2.70	4.92	13.472	1.329	0.133	0.102	0.425
P5(4)	.01	Mg Calcite	-3.33	5.27	9.844	0.975	0.130	0.089	0.131
P5(4)	.02	Mg Calcite	-3.89	4.95	8.578	0.850	0.126	0.096	0.143
P5(4)	.04	Mg Calcite	-2.58	5.25	14.044	1.385	0.131	0.099	0.191
P5(4)	.05	Mg Calcite	-2.43	5.03	11.850	1.171	0.138	0.103	0.354
P7A	.01	Mg Calcite	-2.76	5.64	13.138	1.297	0.155	0.079	0.111
P7A	.02	Mg Calcite	-2.75	5.56	19.665	1.928	0.164	0.070	0.097
P7A	.03	Mg Calcite	-3.52	4.00	11.557	1.142	0.140	0.080	0.161
P7B(1)	.01	Mg Calcite	-2.97	5.31	11.929	1.179	0.132	0.068	0.104
P7B(1)	.02	Mg Calcite	-2.85	5.73	11.542	1.141	0.134	0.067	0.082

$\delta_{18}O$ and $\delta_{13}C$ values are reported in ‰ notation relative to VPDB
Elemental ratios are expressed as mmol/mol